The Astrophysical Journal Letters, 997:L38 (17pp), 2026 February 1 https://doi.org/10.3847/2041-8213/adf06f
© 2026. The Author(s). Published by the American Astronomical Society.
OPEN ACCESS

A Cool Earth-sized Planet Candidate Transiting a Tenth Magnitude K-dwarf From K2

Alexander Venner[1,6], Andrew Vanderburg[2], Chelsea X. Huang[1], Shishir Dholakia[1], Hans Martin Schwengeler[3,6], Steve B. Howell[4], Robert A. Wittenmyer[1], Martti H. Kristiansen[5,6], Mark Omohundro[3,6], and Ivan A. Terentev[3,6]
[1] Centre for Astrophysics, University of Southern Queensland, Toowoomba, QLD 4350, Australia; alexandervenner@gmail.com
[2] Center for Astrophysics, Harvard & Smithsonian, Cambridge, MA 02138, USA
[3] Citizen scientist, c/o Zooniverse, Department of Physics, University of Oxford, Denys Wilkinson Building, Keble Road, Oxford, OX1 3RH, UK
[4] NASA Ames Research Center, Moffett Field, CA 94035, USA
[5] Brorfelde Observatory, Observator Gyldenkernes Vej 7, DK-4340 Tølløse, Denmark
Received 2025 June 9; revised 2025 July 13; accepted 2025 July 16; published 2026 January 27

Abstract

The transit method is currently one of our best means for the detection of potentially habitable "Earth-like" exoplanets. In principle, given sufficiently high photometric precision, cool Earth-sized exoplanets orbiting Sun-like stars could be discovered via single transit detections; however, this has not previously been achieved. In this work, we report a 10 hr long single transit event which occurred on the $V = 10.1$ K-dwarf HD 137010 during K2 Campaign 15 in 2017. This transit is comparatively shallow (225 ± 10 ppm) but is detected at high signal-to-noise thanks to the exceptionally high photometric precision achieved for the target. Our analysis of the K2 photometry, historical and new imaging observations, and archival radial velocities and astrometry strongly indicate that the event was astrophysical, occurred on-target, and can be best explained by a transiting planet candidate, which we designate HD 137010 b. The single observed transit implies a radius of $1.06^{+0.06}_{-0.05}$ $R_\oplus$, and assuming negligible orbital eccentricity we estimate an orbital period of 355^{+200}_{-59} days ($a = 0.88^{+0.32}_{-0.10}$ au), properties comparable to Earth. We project an incident flux of $0.29^{+0.11}_{-0.13}$ $I_\oplus$, which would place HD 137010 b near the outer edge of the habitable zone. This is the first planet candidate with Earth-like radius and orbital properties transiting a Sun-like star bright enough for substantial follow-up observations.

Unified Astronomy Thesaurus concepts: Exoplanet astronomy (486); Exoplanets (498); Extrasolar rocky planets (511); Transit photometry (1709); Exoplanet detection methods (489); Habitable zone (696)

Materials only available in the online version of record: machine-readable table

1. Introduction

The detection of potentially habitable "Earth-like" planets is a major and enduring goal of exoplanet research. At present, planets of Earth-like mass and/or radius orbiting in the circumstellar habitable zone (HZ), where liquid water could potentially exist, lie near to or beyond current sensitivity limits for Sun-like FGK stars. However, out of all exoplanet detection techniques, the transit method has demonstrated particularly high efficacy for the detection of these exoplanets. The search for Earth-sized exoplanets in the HZs of Sun-like stars was the core scientific aim of the Kepler mission (W. J. Borucki et al. 2010; D. G. Koch et al. 2010), which observed a 116 square degree field in the northern sky quasi-continuously for 4 yr. Of its many exoplanet discoveries, Kepler detected the first-known small transiting planets orbiting in the HZ (Kepler-22, W. J. Borucki et al. 2012; Kepler-62, W. J. Borucki et al. 2013; Kepler-452, J. M. Jenkins et al. 2015), including the first "Earth-sized" HZ planet (Kepler-186, E. V. Quintana et al. 2014).[7] However, given that the majority Kepler target stars are faint ($V > 13$), the transits of these planets often lie close to the detection limits for Sun-like stars and the validity of some of these planets has been questioned (F. Mullally et al. 2018; C. J. Burke et al. 2019). This was exacerbated by the premature end of the Kepler mission in 2013 due to instrument failure.

In recent times, much of the focus of transiting exoplanet research has moved to the Transiting Exoplanet Survey Satellite (TESS; G. R. Ricker et al. 2014). Like Kepler before it, TESS has had an immense impact on the study of transiting planets. However, the shorter observing baselines and lower photometric precision of TESS means that it is not optimized for detection of temperate terrestrial planets orbiting Sun-like stars. Earth-sized planets discovered by TESS orbiting FGK-type tend to orbit bright stars with short orbital periods (e.g., D. Dragomir et al. 2019; M. Kunimoto et al. 2025). In contrast, M-dwarfs present an advantage in that the transits of terrestrial planets are proportionally deeper and temperate planets can be found at shorter orbital periods. As a result, temperate terrestrial planets discovered by TESS have exclusively been found in the orbit of M-dwarfs (e.g., TOI-700, E. A. Gilbert et al. 2020, 2023; J. E. Rodriguez et al. 2020; TOI-715, G. Dransfield et al. 2024; Gliese 12, S. Dholakia et al. 2024; M. Kuzuhara et al. 2024); indeed, the detection capabilities of TESS for M-dwarf planets even extend to planets significantly cooler than Earth (e.g., $T_{\rm eq} \approx 200$ K, M. G. Scott et al. 2025). However, equivalent planets orbiting Sun-like stars lie largely beyond the reach of TESS. In the near future, missions such as PLATO (H. Rauer et al. 2014, 2025, expected 2026) and Earth 2.0 (ET; J. Ge et al. 2022, expected 2028) aim to detect Earth-sized planets orbiting in the HZs of Sun-like stars through a Kepler-like "stare" observing strategy. If past Kepler results provide a comparable benchmark, the detection of planets with Earth-like orbital periods will require several years of observations.

[6] Planet Hunters K2 contributors.
[7] For this work, we arbitrarily define "Earth-sized" as being within 25% of the radius of Earth, i.e., $0.8 < R_{\rm p} < 1.25\ R_\oplus$.

Original content from this work may be used under the terms of the Creative Commons Attribution 4.0 licence. Any further distribution of this work must maintain attribution to the author(s) and the title of the work, journal citation and DOI.

Acknowledging this historical context, the K2 mission (S. B. Howell et al. 2014) occupies a unique position in this paradigm. After instrument failures prematurely ended the Kepler prime mission, K2 repurposed the telescope to conduct a transit survey of the ecliptic plane focusing on brighter stars. After implementing corrections to the challenging photometric systematics caused by the spacecraft's motion, K2 observations provided high photometric precision that match Kepler performance, especially for bright stars (e.g., A. Vanderburg et al. 2016a, Section 6.3). In the best of cases, the precision of K2 photometry allowed for the detection of planets with Earth-like transit depths ($\approx$100 ppm), making it potentially sensitive to temperate terrestrial exoplanets.

Since K2 depended on radiation pressure from the Sun for its pointing, the duration of each K2 pointing was restricted to $\lesssim$80 days per campaign. This meant that unlike Kepler, transiting planets with longer orbital periods could not be detected conventionally through repeat transit detections. However, discoveries through observations of single transits does remain a possibility. The study of exoplanets from single transits began in earnest with Kepler (e.g., J. Wang et al. 2015; D. Foreman-Mackey et al. 2016; S. Uehara et al. 2016), was developed further during K2 (e.g., H. P. Osborn et al. 2016), and has become especially opportune in the TESS era (e.g., N. L. Eisner et al. 2021; P. A. Dalba et al. 2022; C. R. Mann et al. 2023; L. A. Sgro et al. 2024). Some notable K2 discoveries based on single transits include the first K2 exoplanet discovery (K2-2; A. Vanderburg et al. 2015; E. Thygesen et al. 2024), the unique planetary system of K2-93 (HIP 41378; A. Vanderburg et al. 2016b), a long-period super-Earth in the Hyades cluster (HD 283869; A. Vanderburg et al. 2018), and what may be the longest-period K2 planet from the extraordinary 54 hr long transit observed on K2-311 (EPIC 248847494; H. A. C. Giles et al. 2018).

Given the high photometric precision attained by K2, there is meaningful potential to detect single-transit events from small long-period exoplanets. For stars smaller than the Sun, including the $\approx$41% plurality of K/M-dwarf K2 targets (D. Huber et al. 2016), this could even extend to Earth-sized planets. Though the book has closed on K2 following the 2018 Kepler end-of-life (S. B. Howell 2020), ongoing study of K2 data continues to bring new discoveries to light (e.g., E. Incha et al. 2023).

In this work, we report the detection of a shallow single transit in K2 observations of the relatively bright K-dwarf HD 137010 ($V = 10.1$). We find that the transit event, which was detected through visual inspection, is best explained by a planet of size ($1.06^{+0.06}_{-0.05}\ R_\oplus$) and orbital period ($355^{+200}_{-59}$ days) comparable to Earth. We estimate that the planet candidate receives a low incident flux, which may place it near the outer edge of the HZ, or potentially even beyond. This is a significant addition to the small sample of cool Earth-sized exoplanets, and presents a small milestone in the search for Earth-like exoplanets around nearby Sun-like stars.

2. Data

2.1. K2 Photometry

HD 137010 (EPIC 249661074) was observed by Kepler for 88 days between 2017 August 23 and 2017 November 19 during Campaign 15 of the K2 mission. Following the method of A. Vanderburg & J. A. Johnson (2014), a systematics-corrected light curve was generated and made available online.[8] Subsequently, one of us (H.M.S.) identified a single-transit-like feature in the light curve through visual inspection using the `LcTools` software (A. R. Schmitt et al. 2019; see M. H. K. Kristiansen et al. 2022). The transit-like feature occurred at BJD$\approx$2458055.1, with a shallow depth of around 225 ppm and a duration of about 10 hr. For this work, we produce a new systematics-corrected light curve from the target pixel files jointly fitting for a transit model (following A. Vanderburg & J. A. Johnson 2014; A. Vanderburg et al. 2016a), which is shown in Figure 1 and tabulated in Appendix A. This event is easily noticed visually thanks to the unusually high precision of the K2 photometry; the 6.5 hr combined differential photometric precision (CDPP) is $\sim$8.5 ppm, close to the limiting dispersion achieved in either Kepler or K2 (ex. R. L. Gilliland et al. 2011; R. Luger et al. 2016). We also observe some low-level variability in the light curve acting at a timescale of weeks, though it is difficult to determine whether this reflects stellar activity or K2 systematics.

Next, we attempt to quantify the statistical significance of the event. We first estimate the signal-to-noise ratio (SNR) of the event assuming classical white Gaussian noise,

$$\mathrm{SNR} = \delta \frac{\sqrt{N}}{\sigma}, \tag{1}$$

where δ is the transit depth, N is the number of in-transit photometric data points, and σ is the standard deviation of the out-of-transit light curve (J. F. Rowe et al. 2014, Section 5.2). In our best-fit transit model (Figure 1), $\delta = 225$ ppm, $N = 18$, and $\sigma = 32$ ppm, which yields SNR = 30. Alternatively, as in M. Kunimoto & J. M. Matthews (2020), we may estimate σ as 1.48$\times$ the median absolute deviation (MAD) of the out-of-transit light curve; here, the MAD is 20 ppm, yielding SNR = 32. This implies high significance for the signal.

A more realistic estimate of the true SNR of the event, taking into account red noise in the light curve, can be obtained by performing a matched filter analysis. Following E. A. Gilbert et al. (2023), we convolved the K2 light curve with the best-fit transit model from our simultaneous fit to the transit and spacecraft systematics. We compared the peak of the matched filter response with the standard deviation of the filter response far from the transit to measure a signal-to-noise ratio of 11.2. If we ignore the first 20 days of the light curve which show slightly higher red noise levels, the SNR of the transit rises above 13. While lower than the white noise SNR, this nonetheless indicates high statistical significance.

We then attempted to evaluate the veracity of the event in the K2 data. To confirm that the event is not simply caused by instrument effects, we inspected the K2 photometry of other stars near to our target. For all stars with K2 observations that lie within 5′ of HD 137010, we do not identify any convincing analogs of the transit-like feature.[9] We also confirmed that the profile and duration of the event is independent of our choice of aperture, consistent with a transit event on the target star.

We next inspected the K2 pixel images to test whether there is any evidence that the event occurred off-target. HD 137010

[8] https://lweb.cfa.harvard.edu/avanderb/k2c15/ep249661074.html

[9] The nearby $V = 12$ star EPIC 249661654 is an eclipsing binary which has an eclipse coincident with the event on HD 137010. However, this eclipse has a shorter duration and a "V-shaped" profile, which is inconsistent with the HD 137010 event. We therefore rule out contamination from this star.

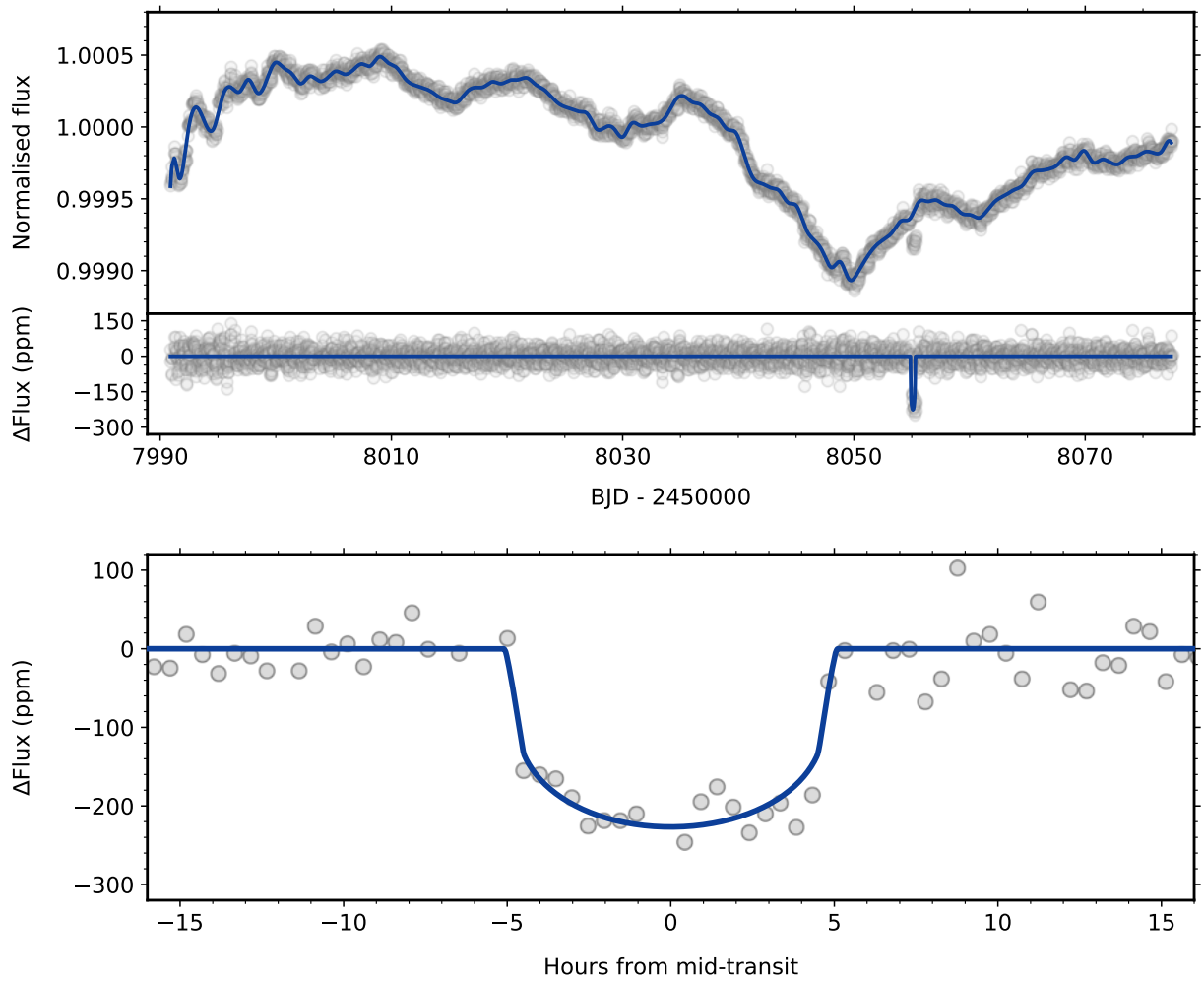


Figure 1. (Top) Systematics-corrected K2 Campaign 15 light curve of HD 137010 (EPIC 249661074). The individual K2 long-cadence flux measurements are marked by gray points, while the blue curve represents a spline model to detrend the long-term photometric variability. A noticeable drop in flux, consistent with a planetary transit, is visible around BJD ≈ 2458055.1. (Middle) K2 light curve with long-term variability removed. A best-fit transit model has been applied to the transit event. (Bottom) Inset focusing on the transit event. The event has a depth of ∼225 ppm and ∼10 hr duration, and we estimate it is detected at a high signal-to-noise of ≈30. The transit event is consistent with an Earth-sized exoplanet with a ≈1 yr orbital period.

is sufficiently bright ($K_p = 9.79$) to significantly saturate Kepler's detector, which makes it challenging to measure the in-transit centroid drift. Nonetheless, we do not observe any coherent changes in the photocentre position during the event at the pixel level. We also do not detect any moving objects in the HD 137010 field around the time of transit, which serves to rule out the possibility that the signal could be caused by a passing solar system object.

We therefore conclude that the event observed in the K2 photometry of HD 137010 is statistically significant and is consistent with having occurred on-target. Furthermore, owing to the high detection significance of the event, we can determine that it possesses a curved flux minimum and short ingress/egress, both of which are typically characteristic properties of a planetary transit.

We return to verify the transit hypothesis in more detail in Section 3.3. If the event is indeed a planetary transit on HD 137010, the 225 ppm depth implies a radius of $\sim 1\,R_{\oplus}$, which would be remarkably small for an object detected from a single transit. In addition, due to the absence of repeat events in the K2 light curve, its orbital period must be longer than >64 days. Estimating the orbital period of a planet from a single transit is challenging, but a first-order estimate can be made by comparison to the orbit of Earth. The idealized duration of the transit of Earth across the Sun is ≈13 hr (R. Heller & R. E. Pudritz 2016), resulting in a transverse velocity across the idealized transit chord of $\sim 3.7\,R_{\odot}$/day. While the observed 10 hr duration of the transit is shorter and implies a transit velocity of $\sim 4.8\,R_{*}$/day, since HD 137010 is a K-dwarf only ∼70% the size of the Sun, this entails a transverse velocity similar to Earth's ($\sim 3.4\,R_{\odot}$/day) if the impact parameter is low. Hence, given the idealized assumptions of low eccentricity and impact parameter, the transit of HD 137010 is consistent with a planet with an Earth-like orbital period ($P \approx 1$ yr). We explore this more rigourously in Section 3.4.

2.2. HARPS Spectroscopy

Independent of the K2 observations, HD 137010 was observed with the HARPS spectrograph (M. Mayor et al. 2003) as part of the volume-limited planet search (G. Lo Curto et al. 2010; S. G. Sousa et al. 2011). This survey was designed to include RV-amenable solar-type stars in the southern hemisphere within a distance of <57.5 pc. Though these observations are not sensitive to the expected RV signal of the

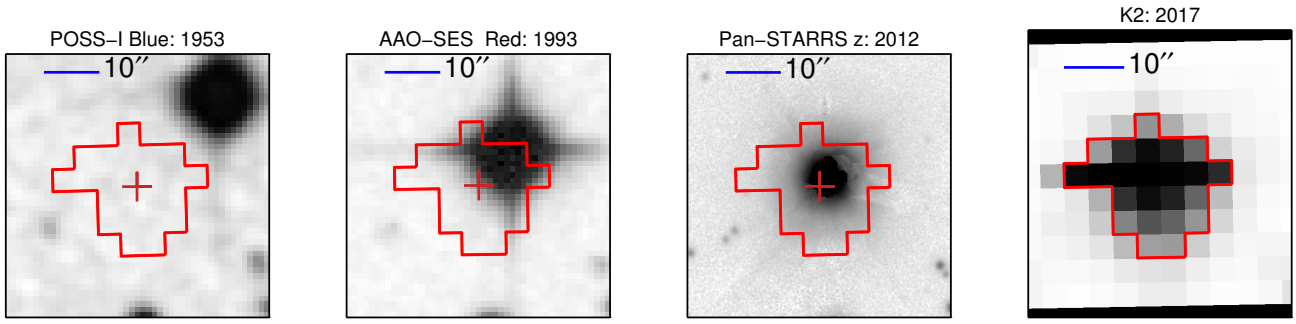


Figure 2. Archival imaging of HD 137010 over time. The location of the star at the epoch of K2 observations is marked by a red cross, and the adopted K2 photometric aperture is shown by the red outline. (Far left) POSS-I blue-wavelength photographic plate image from 1953. (Center left) AAO-SES red-wavelength photographic plate image from 1993. (Center right) Pan-STARRS z-band image from 2012. (Far right) Summed image from K2 observations. We do not observe any background stars brighter than ≈19th magnitude that fall within the K2 photometric aperture, leading us to conclude that background flux contamination is negligible.

transiting planet candidate, they allow us to check for the presence of other companions orbiting the star.

We downloaded the HARPS observations from the ESO Science Archive.[10] HD 137010 was observed with HARPS eight times between 2006 April 9 and 2010 April 21, with a median RV uncertainty of 1.4 m s^{-1}. The observing cadence is discontinuous, given that the first four observations date to 2006 whereas the latter four belong to 2010. The HARPS RVs do not show any evidence of short-term RV variability, which might occur in false-positive scenarios. However, there is a ≈7 m s^{-1} offset between the 2006 and 2010 RVs, which is too large and has too long of a timescale to plausibly be attributed to the transiting planet candidate. We return to explore this variability in Section 3.2. Normalizing for the offset between the 2006 and 2010 RVs, we find that the rms of the RVs is 1.3 m s^{-1}, which is on par with the RV uncertainties. We therefore conclude that the available RV data do not contradict the planetary hypothesis. We reproduce the HARPS RVs in Appendix A.

2.3. Hipparcos–Gaia Astrometry

HD 137010 has been observed by both Hipparcos (HIP 75398; M. A. C. Perryman et al. 1997) and Gaia (Gaia Collaboration et al. 2016). This allows us to use Hipparcos–Gaia astrometry to constrain the tangential motion of the star over the 25 yr inter-mission baseline. We extract the astrometric data from the Gaia EDR3 version of the Hipparcos–Gaia Catalog of Accelerations (HGCA; T. D. Brandt 2018, 2021). We reproduce this data in Appendix A. There is no significant evidence for an astrometric acceleration in the Hipparcos–Gaia astrometry; the offset between the Gaia proper motion and the Hipparcos–Gaia mean proper motion is $\Delta\mu = (-0.003 \pm 0.074, +0.025 \pm 0.053$ mas yr$^{-1})$ in R.A. and decl., respectively, equivalent to $\Delta v = (-1 \pm 16, +5 \pm 11$ m s$^{-1})$ in SI units (A. Venner et al. 2021, Equations (9), (10)). We therefore set a 3σ upper limit of $\Delta v < 47$ m s^{-1} on the net Hipparcos–Gaia tangential velocity anomaly, excluding large variations in the stellar motion over the Hipparcos–Gaia observing interval.

[10] https://archive.eso.org/wdb/wdb/adp/phase3_spectral/form?phase3_collection=HARPS

2.4. Imaging

Imaging observations can be used to search for comoving stellar companions as well as background sources which may contaminate observations of HD 137010. In particular, the star has a relatively large proper motion of 340 mas yr^{-1} (Gaia Collaboration et al. 2023), making it possible to use archival imaging observations to constrain the existence of background stars within the 2017 K2 photometric aperture.

In Figure 2, we show a sequence of imaging observations ranging from 1953 through to the 2017 K2 observations, with the K2 photometric aperture shown to scale. The two nearest visible background stars to HD 137010, visible at ≈20″ separation toward the lower left of the frame in Figure 2, are detected in Gaia DR3 with G-band magnitudes of 19.4 (Gaia DR3 6254679268787107584) and 20.7 (Gaia DR3 6254679273084416000). Given that these sources are visible in all of the archival imaging, we estimate that these images would be able to detect background stars brighter than ≈19th magnitude within the K2 photometric aperture. However, no such background stars are visible in any of the archival images. We can therefore exclude the existence of any background sources with a flux contrast below $\Delta \lesssim 9$ mag that contaminate the K2 photometry.

We obtained new high-resolution speckle imaging observations of HD 137010 to check for close-separation stellar companions that would be unresolved in the previously discussed imaging data (J. R. Schmitt et al. 2016). We used the Zorro speckle instrument at the Gemini South Telescope (N. J. Scott et al. 2021; S. B. Howell et al. 2025) to obtain high-contrast speckle imaging data on 2024 July 12. Observations were taken in two medium-band filters with central wavelengths of 562 nm and 832 nm, respectively, with a total field of view of $2.8 \times 2.''8$. We reduced the imaging data following methods described in S. B. Howell et al. (2011, 2016). We reproduce the reconstructed image and contrast limits in Appendix A. Our observations achieve a contrast limit of $\Delta = 5$ mag at $0.''1$ separation, through to $\Delta = 7$–8 mag around $1''$. The multiband detection limits exclude contaminants with spectral types later than ≳A0 at $0.''1$ and ≳M0 at $1''$.

We do not detect any additional stars in the speckle imaging field. However, since the speckle imaging epoch postdates the K2 observations by approximately 7 yr, HD 137010 will have moved by over $>2''$ in the intervening time and our new imaging observations would not capture background sources

Table 1
Properties of HD 137010

Parameter	Value	References
R.A. α_{J2000} …	15:24:21.25	Gaia Collaboration et al. (2023)
decl. δ_{J2000} …	−19:44:21.68	Gaia Collaboration et al. (2023)
V (mag) …	10.14 ± 0.05	E. Høg et al. (2000)
K_p (mag) …	9.79	D. Huber et al. (2016)
Parallax ϖ (mas) …	22.292 ± 0.017	Gaia Collaboration et al. (2023)
Distance (pc) …	44.86 ± 0.03	Gaia Collaboration et al. (2023)
R.A. proper motion μ_α (mas yr^{-1}) …	+228.536 ± 0.021	Gaia Collaboration et al. (2023)
Decl. proper motion μ_δ (mas yr^{-1}) …	−248.158 ± 0.014	Gaia Collaboration et al. (2023)
Radial velocity (km s^{-1}) …	+27.866 ± 0.001	C. Soubiran et al. (2018)
U (km s^{-1}) …	+59.18 ± 0.03	This work
V (km s^{-1}) …	−11.16 ± 0.01	This work
W (km s^{-1}) …	−47.83 ± 0.05	This work
Spectral type …	K3.5V	R. O. Gray et al. (2006)
$\log R'_{HK}$ …	−4.84	J. Gomes da Silva et al. (2021)
[Fe/H] (dex) …	−0.22 ± 0.07	S. G. Sousa et al. (2011)
$T_{\rm eff}$ (K) …	4770 ± 90	This work
M_* ($M_\odot$) …	0.726 ± 0.017	This work
R_* ($R_\odot$) …	0.707 ± 0.023	This work
ρ_* (g cm^{-3}) …	$2.90^{+0.29}_{-0.26}$	This work
log$g$ (cm s^{-2}) …	4.60 ± 0.03	This work
L_* ($L_\odot$) …	$0.232^{+0.023}_{-0.021}$	This work
Age (Gyr) …	4.8 − 10	This work

located in the K2 aperture. Nonetheless, the speckle imaging is informative for excluding comoving companions to HD 137010. We explore this further in Section 3.2.2.

In summary, we find that there is no evidence for either background sources or comoving companion stars that could have interfered with or contaminated the K2 photometry.

3. Analysis

3.1. Stellar Properties

HD 137010 is a $V = 10.1$ mag star with a spectral type of K3.5V (R. O. Gray et al. 2006), located at a distance of 44.86 ± 0.03 pc in the constellation Libra (J2000 R.A. and decl. = 231.0885 −19.7394; Gaia Collaboration et al. 2023). In the following we recount the relevant physical properties of the star. We also summarize the most salient of these parameters in Table 1.

3.1.1. Kinematics and Age Estimation

We first turn to the age of the system. HD 137010 is appreciably subsolar in mass, so its main sequence lifetime is longer than the age of the Universe and its rate of evolution is sufficiently slow that stellar isochrone models are not strongly age-sensitive. To get a sense for the age of the star, we therefore first consider its kinematics.

Based on the Hipparcos astrometric solution and the absolute RV measured by HARPS, V. Z. Adibekyan et al. (2012) calculate space velocities of $(U_{\rm LSR}, V_{\rm LSR}, W_{\rm LSR})$=(+64, +2, −30) km s^{-1}, where U is positive in the direction of the galactic center, V is positive toward the galactic rotation, and W is positive in the direction of the north galactic pole. Using the methods for assignation of stars to galactic populations from T. Bensby et al. (2003) and A. C. Robin et al. (2003), respectively, V. Z. Adibekyan et al. (2012) report an 89% or 95% probability that HD 137010 belongs to the thin disk, with the remainder entailing assignment to the thick disk. There is therefore a high probability that this star belongs to the younger component of the galactic disk. There is a consensus that the thin disk began to form ≈8–10 Gyr ago (K. Fuhrmann 2011; M. Xiang et al. 2017), so membership of HD 137010 in this population implies an age below <10 Gyr.

We recalculate the relative space velocities of HD 137010 following D. R. H. Johnson & D. R. Soderblom (1987), using newer positions and proper motions from Gaia DR3 and the radial velocity from the C. Soubiran et al. (2018) catalog of Gaia radial velocity standards (data reproduced in Table 1). For the conversion between equatorial and galactic coordinates, we use the Hipparcos transformation matrix, also utilized in Gaia DR3.[11] We find $(U, V, W) = (+59.18 \pm 0.03, -11.16 \pm 0.01, -47.83 \pm 0.05)$ km s^{-1}. Adopting the solar space velocities from R. Schönrich et al. (2010), we find absolute motions relative to the local standard of rest $(U_{\rm LSR}, V_{\rm LSR}, W_{\rm LSR}) = (+70.3 \pm 0.8, +1.1 \pm 0.5, -40.6 \pm 0.4)$ km s^{-1}. These values stand in reasonable agreement with those of V. Z. Adibekyan et al. (2012), though $V_{\rm LSR}$ and $W_{\rm LSR}$ differ fairly substantially; the difference can mainly be attributed to the Hipparcos parallax, which is larger than the Gaia value but relatively imprecise ($\varpi_{\rm HIP} = 26.65 \pm 2.65$ mas; F. van Leeuwen 2007).

Comparison with the stellar sample of (V. Z. Adibekyan et al. 2012, Figure 6) is sufficient to reconfirm that the star most likely belongs to the thin disk. However, the kinematics of HD 137010 are comparatively hot for a thin-disk member. Our value for the total velocity, $v_{\rm tot} \equiv \sqrt{U_{\rm LSR}^2 + V_{\rm LSR}^2 + W_{\rm LSR}^2} \approx 81$ km s^{-1}, is notably high for a thin-disk star. To better quantify the age implied by its kinematics, we use the *UVW*-age relationships of F. Almeida-Fernandes & H. J. Rocha-Pinto (2018) and M. J. Veyette & P. S. Muirhead (2018) to estimate the kinematic age of HD 137010. These are calibrated to Sun-like thin-disk stars in the solar neighborhood with known isochrone ages.

Using these velocity-age relationships, we find nominal ages of $T = 9.3^{+3.0}_{-3.2}$ Gyr and $T = 10.4^{+2.2}_{-2.4}$ Gyr respectively. These values abut with the upper limit on the age of the thin disk, clearly supporting an old age for the star. Given that these posteriors also lie at the maximal extreme of the calibration of the velocity-age relationship (i.e., being limited to thin-disk stars with ages below <10 Gyr; F. Almeida-Fernandes & H. J. Rocha-Pinto 2018), we opt to use the lower limits provided by the relations. The corresponding 3σ lower limits are $T > 2.6$ Gyr and $T > 4.8$ Gyr, respectively; we prefer to adopt the latter of these values because this relation is less skewed toward young ages (M. J. Veyette & P. S. Muirhead 2018). We therefore adopt a broad age constraint for HD 137010 of [4.8, 10] Gyr from its kinematics.

[11] See Section 4.1.7 (Equation (4).62) of the Gaia DR3 documentation https://www.cosmos.esa.int/web/gaia-users/archive/gdr3-documentation).

An old age for the star is consistent with the low level of observed stellar activity. R. O. Gray et al. (2006) report $\log R'_{HK} = -4.96$ from their spectral observations of HD 137010, whereas J. Gomes da Silva et al. (2021) have more recently reported a mean $\log R'_{HK} = -4.84$ from the HARPS spectra. This implies a low level of magnetic activity, as expected for a Sun-like star of supersolar age.

3.1.2. Stellar Fundamental Parameters

Having established constraints on the age of HD 137010, we next use stellar models to determine its remaining properties. We use the MIST isochrones (J. Choi et al. 2016; A. Dotter 2016) to model the physical parameters of HD 137010, using a model applied in our previous work (A. Venner et al. 2024). We provide details of the data and priors used for our isochrone model in Appendix B. The photometry we have used in our model includes space-based photometry from Tycho-2, Gaia, 2MASS, and WISE which spans optical and infrared wavelengths. We adopt spectroscopic priors of $T_{\rm eff} = 4797 \pm 121$ K and [Fe/H] $= -0.22 \pm 0.07$ dex as determined from the HARPS data by S. G. Sousa et al. (2011). We also use constraints from the preceding section as age priors.

Our isochrone model returns a stellar mass of $0.726 \pm 0.017\,M_\odot$ and radius $0.707 \pm 0.023\,M_\odot$, in line with expectations for a K3.5V star. This scales to a density of $2.90^{+0.29}_{-0.26}$ g cm^{-3} and $\log g$ of 4.60 ± 0.03 (surface gravity of $10^{4.60\pm0.03}$ cm s^{-2}). We find a posterior effective temperature of 4770 ± 90 K, which coupled with the stellar radius results in a bolometric luminosity of $0.232^{+0.023}_{-0.021}\,L_\odot$ using the Stefan–Boltzmann law. We summarize the key stellar parameters in Table 1.

3.2. Limits on Additional Companions

We next attempt to place constraints on the existence of additional bodies in the system. This includes placing limits on additional transiting planets in the K2 light curve, and attempting to constrain the existence of additional companions on external orbits using other data.

3.2.1. Constraints on Additional Transiting Planets

We first search for additional transit signals in the K2 photometry. We use the Box Least Square algorithm (BLS; G. Kovács et al. 2002) implemented in the `Vartools` package (J. D. Hartman & G. Á. Bakos 2016) to search the light curve time series, with the single transit masked out. We search for planets with period between 0.3 and 60 days, with 150,000 bins in frequency space. We do not detect any signals with a BLS signal-to-pink-noise ratio above $\geqslant$9, indicating there are no periodic transit signals from additional planets detectable in the light curve.

We then perform an injection and recovery analysis to estimate the parameter space of transiting planets that could be detected in the K2 photometry. For each iteration of the injection and recovery, we simulate the transits of a planet with radii drawn from a uniform distribution between 0.3 and 4 $R_\oplus$, orbital periods drawn from a uniform distribution between 0.5 and 50 days, impact parameter uniformly distributed between 0 and 0.9, and a random orbital phase. The transit signal of the simulated planet is then injected to the systematics-corrected K2 light curve (Figure 1, top panel) with the known transit signal masked out. We then use a Basis Spline (A. Vanderburg et al. 2016b) to detrend the light curve before performing the same BLS search described previously. The injected planet is defined as recovered if it is detected with a BLS signal-to-pink-noise above >9, and with a period and epoch matching the originally injected signal following the algorithms described in J. L. Coughlin et al. (2014). We repeat the injection and recovery for 20,000 iterations to sample across the period and radius parameter space. We present the distribution of detectability fractions in Figure 3. Given the extremely high precision of the K2 light curve, we achieve an exceptionally high detectability completeness for planets larger than $>1\,R_\oplus$, and can effectively rule out the existence of any additional transiting planets larger than Earth orbiting HD 137010 with orbital periods below <30 days. Toward smaller planetary radii our sensitivity declines, though we may nonetheless largely exclude planets larger than Mars ($>0.5\,R_\oplus$) with orbital periods shorter than <15 days. For orbital periods beyond >30 days, our detectability fractions begin to decline across the board, with the detection efficiency being limited by the 88 day duration of the K2 light curve. We conclude that there is no evidence for additional transiting planets as large as HD 137010 b in the K2 photometry.

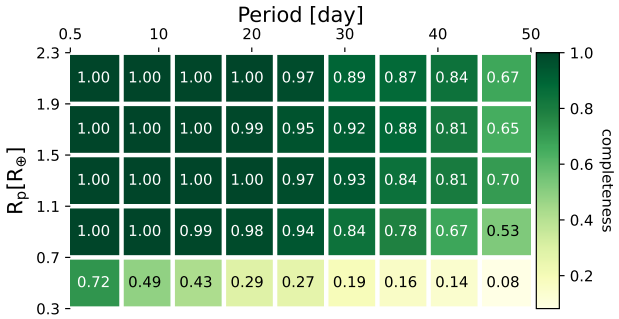


Figure 3. Detectability fractions for transiting planets injected into the K2 light curve across various orbital periods and radii. Owing to the high photometric precision, we are able to almost entirely exclude transiting planets larger than $>1\,R_\oplus$ with orbital periods shorter than <30 days.

3.2.2. Constraints on Companions on Wider Orbits

We next attempt to place constraints on tertiary companions orbiting exterior to the detected transiting planet candidate. In Section 2.4, we used our speckle imaging observations to put limits on the existence of stellar companions between projected separations of 0.″1 and 1″ (=5–45 au). Based on the 832 nm contrast limits, we estimate that within this range we can rule out stellar companions more massive than $\gtrsim$0.15 $M_\odot$ beyond a projected separation of >0.″1 (>5 au), and $\gtrsim$0.1 $M_\odot$ beyond >0.″6 (>25 au).

To extend our companion limits beyond >1″, we use data from Gaia DR3 (Gaia Collaboration et al. 2023). Empirically, Gaia is sensitive to binaries with $\Delta G \approx 4$ mag contrast at 1″ separation and $\Delta G \approx 7$ mag at 2″, with sensitivity continuing to improve thereafter (K. El-Badry et al. 2021, Figure 9). Gaia has detected no other sources within 10″ of HD 137010. This effectively rules out stellar companions more massive than $\gtrsim$0.25 $M_\odot$ at 1″ (45 au projected) and companions above $\gtrsim$0.15 $M_\odot$ beyond >2″ (>90 au). We do not find any stars in Gaia DR3 which share distance and proper motion within 10′ of HD 137010.

To further expand our sensitivity to wide companions, we next consider constraints from the HARPS RVs and the Hipparcos–Gaia astrometry. We do not observe any significant evidence for an acceleration in the astrometry, but in the HARPS data we do see a $\approx 7\,\mathrm{m\,s^{-1}}$ offset between the 2006 and 2010 observations. Given the limited scope of the HARPS data set, it is difficult to evaluate the origin of this drift. However, we note that the amplitude and timescale are too large to be explained by the transiting planet candidate, and we do not observe a correlation between the RVs and the width of the line bisectors that might indicate an origin from stellar activity. We therefore consider the possibility that the drift in the HARPS RVs could originate from an additional companion orbiting HD 137010.

Given that we have constraints on both the radial and tangential velocity change for the star, it is possible to compute companion masses as a function of velocity change and projected separation. The relevant expression for companion mass M (in M_J) is

$$M = 5.599 \times 10^{-3} \times D^2 \times \rho^2 \times \left(\frac{d\mathrm{TV}}{dt}\right)^{-2} \times \left[\left(\frac{d\mathrm{RV}}{dt}\right)^2 + \left(\frac{d\mathrm{TV}}{dt}\right)^2\right]^{\frac{3}{2}}, \quad (2)$$

where D is the stellar distance in parsecs, ρ is the projected separation in arcseconds, RV represents the radial velocity, and TV the tangential velocity $=\sqrt{\mu_\alpha^2 + \mu_\delta^2}$ (B. P. Bowler et al. 2021, Equation (2); and see further T. D. Brandt et al. 2019, Section 5). Since D is known from Gaia parallax, we can convert from the observed acceleration terms into companion masses as a function of projected separation (for this see also M. Kunimoto et al. 2025).

We perform a simple fit to the RVs and astrometry using linear acceleration terms. Using this model, we find acceleration terms of $\frac{dRV}{dt} = +1.7 \pm 0.4\ \mathrm{m\,s^{-1}\,yr^{-1}}$, $\frac{d\mu_\alpha}{dt} = 0.0 \pm 1.3\ \mathrm{m\,s^{-1}\,yr^{-1}}$, and $\frac{d\mu_\delta}{dt} = +0.4 \pm 1.0\ \mathrm{m\,s^{-1}\,yr^{-1}}$; we plot the best-fit linear acceleration solutions in Figure 4. The radial acceleration is nominally significant at above $>4\sigma$ confidence; however, the time baseline of the HARPS RVs is substantially less than the Hipparcos–Gaia astrometry (4 yr versus 25 yr), so it is not currently possible to demonstrate that the acceleration is linear over long timescales. The method we are using here relies on the assumption that the accelerations are effectively instantaneous (T. D. Brandt et al. 2019), which is uncertain in this case. We therefore advise caution in interpreting these results.

Assuming that a linear acceleration model is valid, we find that the companion mass lies under the canonical deuterium-burning limit ($<13\,M_J$) for projected separations below $\lesssim$20 au, and under the hydrogen-burning limit ($\lesssim 75\,M_J$) within $\lesssim$50 au. The absence of any larger acceleration in the RVs and astrometry thoroughly rule out any stellar-mass companions interior to $<$30 au. Given that our speckle imaging rules out companions above $\gtrsim 0.1\,M_\odot$ between 25 and 45 au, and Gaia can exclude companions more massive than $\gtrsim 0.15\,M_\odot$ beyond $>$90 au, we can reject the existence of all but the least massive stellar companions to HD 137010 at all projected separations. This strongly suggests that HD 137010 is a single star, and severely constrains the possible parameter space for stellar companions that could contaminate the K2 photometry.

3.3. Signal Interpretation

For exoplanet candidates that have only been detected through transit observations, care must be taken to rule out various false-positive scenarios involving architectures without planets that could equally reproduce the photometry. There are now well-established guidelines for the statistical validation of transiting planets (e.g., A. Vanderburg et al. 2019). We consider the following false-positive hypotheses which could potentially reproduce the observed transit of HD 137010:

1. On-target eclipsing binary (EB) If the observed transit signal were caused by the eclipse of HD 137010 by a bound stellar companion, we would expect a large (several $\mathrm{km\,s^{-1}}$) reflex velocity signal corresponding to a binary orbit of a few years. No such variability is detected, with both the RVs and astrometry being stable at the level of a few $\mathrm{m\,s^{-1}}$. We can therefore exclude this hypothesis.
2. Nearby or background EB: An unassociated EB could be the source of the transit if it lies sufficiently close to HD 137010. Though the K2 photometric aperture is extended due to saturation of the target star ($\approx$20″–30″), our analysis of the pixel images suggests that it is unlikely that the transit centroid offset is much larger than a Kepler pixel ($\lesssim$4″; Section 2.1). Using archival imaging, we have ruled out background sources with a contrast below $\Delta \lesssim 9$ mag at the K2 epoch (Section 2.4). If the transit did originate from a blended EB, the observed depth would follow

$$\delta_{\mathrm{obs}} = \delta_{\mathrm{EB}} \frac{f_{\mathrm{EB}}}{f_{\mathrm{total}}}, \quad (3)$$

   where δ is the transit depth as a proportion of total flux, f_{EB} is the total flux of the blended EB, and f_{total} is the combined flux of the target and blend (A. Vanderburg et al. 2019, Equation (1); M. Kunimoto et al. 2025, Equation (2)). We can convert from magnitude contrast Δm to flux ratio following $(f_{\mathrm{EB}}/f_{\mathrm{total}}) = 10^{-0.4\Delta m}$. Given $\delta_{\mathrm{obs}} = 225$ ppm and $\Delta m > 9$ mag, blending with an undetected EB would entail $\delta_{\mathrm{EB}} > 90\%$ at minimum, i.e., quasi-total eclipse of the source. However, such a deep eclipse would require a large occulter which would produce a "V-shaped" transit profile, inconsistent with the "U-shaped" transit we observe. We can therefore reject the background EB hypothesis.
3. Hierarchical triple: This scenario requires a blended EB that is gravitationally bound to the system. Due to the absence of a significant centroid shift, we would still require that the EB lies within $\lesssim$4″ ($\lesssim$200 au projected separation). The absence of any large acceleration in the HARPS RVs and Hipparcos–Gaia astrometry rule out any stellar-mass companions within $\lesssim$0.7″ (Section 3.2.2). Between 0.″6 and 1″, our speckle imaging rules out companions above $\gtrsim 0.1\,M_\odot$; Gaia excludes companions above $\gtrsim 0.25\,M_\odot$ between 1″ and 2″, and above $\gtrsim 0.15\,M_\odot$ beyond $>$2″. This severely restricts the potential parameter space for undetected stellar companions, but does not rule them out entirely. However, we

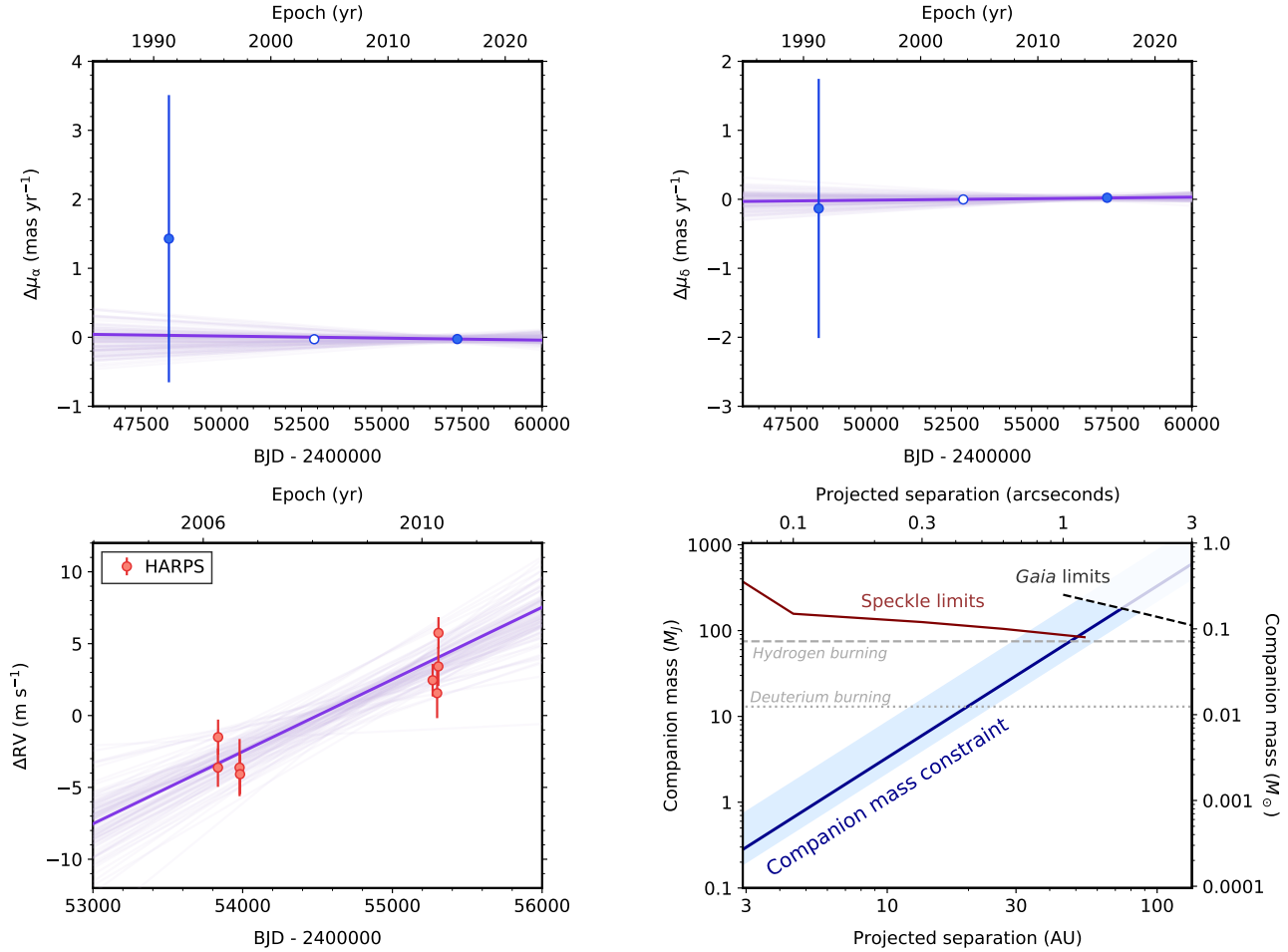


Figure 4. Linear acceleration model for HD 137010 in Hipparcos–Gaia astrometry (R.A., top left; decl., top right), and radial velocity (bottom left; note different axes). The radial acceleration is nominally over $>4\sigma$ from zero ($+1.7 \pm 0.4$ m s^{-1} yr^{-1}), which may suggest the existence of a third body in the system, while the astrometric accelerations are not significant. We estimate the implied companion mass as a function of projected separation (bottom right). The RV acceleration may be explained by a planetary-mass companion within $\lesssim$20 au, or a brown dwarf within $\lesssim$50 au; most stellar companions are excluded by imaging nondetections. However, the limited HARPS data set prevents us from determining whether the acceleration is truly linear, so further observations are necessary to understand the RV variation.

may still rule out the hierarchical triple hypothesis using information from the transit shape:

$$\delta_{\rm EB} \leqslant \frac{(1 - t_{\rm F}/t_{\rm T})^2}{(1 + t_{\rm F}/t_{\rm T})^2}, \tag{4}$$

where $t_{\rm T}$ is the total transit duration (first to fourth contact) whereas $t_{\rm F}$ is the transit duration excluding ingress and egress (second to third contact;M. Kunimoto et al. 2025, Equation (3), see, A. Vanderburg et al. 2019, Equation (2)). We may then insert this into Equation (3) to derive a lower limit on the flux contrast for hierarchical triples that could reproduce the observed transit. In our case, all we can empirically prove is that transit ingress/egress is not clearly resolved in the 29.4 minutes cadence of the K2 photometry (Figure 1); we set $t_{\rm T} = 10$ hr and $t_{\rm F} = 9$ hr to allow for a $\sim$30 minutes ingress/egress, which result in $\Delta m < 2.7$ mag. Given the Kepler-band $K_p = 9.79$ of HD 137010, this would require the blended companion to be brighter than $K_p > 12.5$, which at the system distance corresponds to a $\gtrsim$M0V companion more massive than $\gtrsim$0.5 $M_\odot$. Given that we have already ruled out such massive stellar companions at all separations, we can reject the hierarchical triple hypothesis.

In conclusion, we find that none of the classical false-positive scenarios for transit signals can be invoked to explain the transit observed on HD 137010. It is customary at this point to quantify a false-positive probability for the transit signal using tools for statistical validation, but this is not possible in this case since we have only a single transit event to work with. Nonetheless, the only further evidence required by the transiting planet hypothesis is periodic repetition of transits. Though we cannot prove that these occur for HD 137010 due to our limited data, there is equally no hypothesis other than a planetary transit that can reasonably explain the event. We therefore consider the transit signal observed on HD 137010 to originate from a planet candidate (sensu A. Vanderburg et al. 2018), which we henceforth refer to as HD 137010 b.

3.4. Transit Model

While confirmation of the exoplanet candidate HD 137010 b is not currently possible within the limitations of the available data, we may still provisionally investigate its properties

through a more involved analysis of the observed transit. Modeling of planets detected from single transits presents a unique challenge in that we do not possess an input constraint on the orbital period, upon which several of the other transit parameters depend. However, the orbital period can be estimated from the transit duration when assuming a prior on the stellar density and orbital eccentricity (e.g., E. Sandford et al. 2019). Whereas one approach is to fit for the transit duration and use this to estimate the period, we opt to directly fit for the period while applying the D. Kipping (2018) single-transit probability prior. This allows us to simultaneously weight against solutions with orbital periods too short to reproduce the long transit duration and solutions with long-period orbital configurations less likely to be observed in transit.

For the purposes of our transit model, we make an assumption of zero orbital eccentricity. Since we have only one transit of HD 137010 b, we must effectively constrain two physical parameters (period, eccentricity) from the transit duration, which is also substantially dependent on the impact parameter; hence, some amount of prior information is necessary. Evidence from the Kepler sample suggests that small planets preferentially have low orbital eccentricities (S. R. Kane et al. 2012); however, this group is skewed toward short orbital periods less analogous to HD 137010 b. Though eccentricity information for longer-period terrestrial planets is limited, low eccentricities do appear to be common. In the solar system, the orbital eccentricities of the terrestrial planets range between 0.007 (Venus) and 0.206 (Mercury). Recently, D. Kipping et al. (2025) have investigated the eccentricity distribution of a small sample of transiting exoplanets and candidates with Earth-like radii and incident fluxes orbiting KM-type stars, and found that the mean eccentricity of the sample is likely to be small ($\leqslant$0.15). To first order, the effect of increasing orbital eccentricity on the transit duration is an increase in the uncertainty on the orbital period as the transit velocity diverges from the mean orbital velocity. However, in our case the uncertainty on the orbital period is already large due to our poor constraint on the transit impact parameter; for small orbital eccentricities ($\lesssim$0.2), the impact on the orbital period uncertainty is not larger than the uncertainty arising from the impact parameter. We therefore make the simplifying assumption that HD 137010 b has zero orbital eccentricity. If the orbital period of HD 137010 b can be further constrained in the future, it may become possible to validate this assumption.

For our transit model we use the `batman` package (L. Kreidberg 2015), which implements the K. Mandel & E. Agol (2002) analytic transit model. To account for the 29.4 minutes Kepler long-cadence integration time, we super-sample our model by a factor of 10. As variables in the model, we fit for the stellar mass M_* and density ρ_*, transit time T_0, orbital period P, impact parameter b, planet-to-star radius ratio R_p/R_*, and quadratic limb darkening coefficients u_1 and u_2. We fit T_0, b, u_1, and u_2 uniformly, whereas all other variables are fitted log-uniformly. Furthermore, we apply Gaussian priors on the stellar mass and density using the posteriors from our isochrone model ($\log M_* = -0.139 \pm 0.010$, $\log \rho_* = 0.462 \pm 0.041$; see Table 1) and priors on the limb darkening coefficients derived from the A. Claret (2018) models in the Kepler bandpass ($u_1 = 0.60 \pm 0.07$, $u_2 = 0.12 \pm 0.07$).

Table 2
Parameters of HD 137010 b from Our Transit Model

Parameter	Value
Transit midtime T_0 (BJD) …	$2458055.0969^{+0.0035}_{-0.0032}$
Transit duration T_D (hr) …	$9.76^{+0.21}_{-0.18}$
Impact parameter b …	<0.85 (3σ)
Relative transit velocity R_* day^{-1} …	$4.76^{+0.23}_{-0.65}$
Transit depth δ (ppm) …	225 ± 10
Radius ratio R_p/R_* …	$0.01368^{+0.0006}_{-0.0004}$
Linear limb darkening u_1 …	0.56 ± 0.07
Quadratic limb darkening u_2 …	0.10 ± 0.07
Orbital period P (days) …	355^{+200}_{-59}
Semimajor axis a (au) …	$0.88^{+0.32}_{-0.10}$
Semimajor axis ratio a/R_* …	270^{+93}_{-37}
Orbital inclination i (°) …	$>89.82^{+0.05}_{-0.03}$ (3σ)
Transit velocity (km s^{-1}) …	$27.0^{+1.8}_{-3.6}$
Radius R_p ($R_\oplus$) …	$1.06^{+0.06}_{-0.05}$
Incident flux I ($I_\oplus$) …	$0.29^{+0.11}_{-0.13}$
Equilibrium temperature ($T_{\rm eq}$) for $\alpha = 0.0$ …	205^{+17}_{-28}
Equilibrium temperature ($T_{\rm eq}$) for $\alpha = 0.3$ …	188^{+16}_{-25}
Equilibrium temperature ($T_{\rm eq}$) for $\alpha = 0.5$ …	173^{+14}_{-23}

We use the Markov Chain Monte Carlo ensemble sampler `emcee` (D. Foreman-Mackey et al. 2013) to explore the parameter space. A total of 50 walkers were used to sample our nine parameter model. The posterior space is substantially non-Gaussian, especially in orbital period, and we found that large chain lengths were required to reach a satisfactory degree of convergence. We opted to set a fixed upper limit on the orbital period of $P < 2000$ d, which we may justify a posteriori because such long periods are improbable when allowed, but significantly hinder convergence of the model. Our final model was run for a total of 1×10^8 steps, requiring about 1 day of computing time. To derive our posterior samples, we discarded the first half of the chain as burn-in and saved every hundredth step across each of the walkers.

We present our posterior values for the planetary parameters of HD 137010 b in Table 2. We report the medians and 68.3% confidence intervals, except for the poorly constrained impact parameter b for which we report our 3σ upper limit (<0.85, where the mode of the posterior is $b = 0$), and a corresponding lower limit on the orbital inclination. We determine that the transit midtime occurred at $T_0 = 2458055.0969^{+0.0035}_{-0.0032}$ BJD, had a total duration of $T_D = 9.76^{+0.21}_{-0.18}$ hr, and entailed a radius ratio of $R_p/R_* = 0.01368^{+0.0006}_{-0.0004}$. Combining these parameters, we may derive the transverse velocity of HD 137010 b during transit using the Equation

$$v_{\rm tr} = \frac{2\sqrt{(1 + R_p/R_*)^2 - b^2}}{T_D}, \quad (5)$$

in relative units of R_*/day (H. P. Osborn et al. 2016, Equation (1)). We therefore derive a transverse velocity during transit of $4.76^{+0.23}_{-0.65}\,R_*$/day, which converts to $27.0^{+1.8}_{-3.6}$ km s^{-1} in absolute units when accounting for the stellar radius. The posterior uncertainties on this value are largely generated by the uncertainties on the impact parameter, which also drives the asymmetric confidence interval. Within the uncertainties, the transit velocity of HD 137010 b is intermediate to the mean

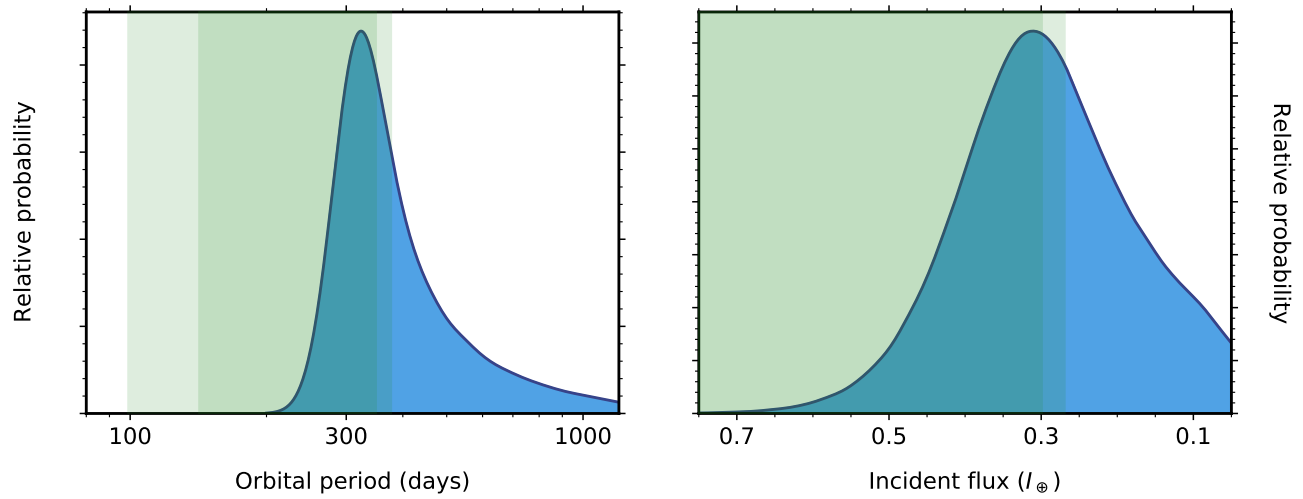


Figure 5. Selected confidence intervals derived from our model for the single transit of HD 137010 b. (Left) Orbital period (355^{+200}_{-59} days). (Right) Stellar flux incident on the planet relative to the Earth equivalent ($0.29^{+0.11}_{-0.13}\,I_\oplus$). We overplot the conservative (dark green) and optimistic (pale green) HZ limits calculated following R. K. Kopparapu et al. (2013). We find that 40% and 51% of our models include HD 137010 b in the conservative and optimistic HZs, respectively.

orbital velocities of Earth and Mars in the solar system (30 km s^{-1} and 24 km s^{-1} respectively), suggesting a comparable orbital separation.

Informed by the stellar mass and density, we ultimately estimate an orbital period of 355^{+200}_{-59} d for HD 137010 b, with a mode of ≈323 days. Emphasizing our assumption of zero orbital eccentricity, shorter orbital periods are rendered improbable since they cannot reproduce the 10 hr transit duration even as $b \to 0$, whereas longer orbital periods are mainly penalized by the $\propto P^{-5/3}$ scaling of the D. Kipping (2018) single-transit probability prior. As for the transit velocity, much of the remaining posterior uncertainty on the orbital period originates from the uncertain impact parameter. From the orbital period of HD 137010 b, we derive a semimajor axis $a = 0.88^{+0.32}_{-0.10}$ au and a relative semimajor axis $a/R_* = 270^{+93}_{-37}$. Compared to the solar system planets, these orbital properties are most similar to Earth.

The observed transit depth of HD 137010 b is only 225 ± 10 ppm, resulting in the aforementioned planet-to-star radius ratio of $0.01368^{+0.0006}_{-0.0004}$. Given the stellar radius of $0.707 \pm 0.023\,R_\odot$, we therefore derive a planetary radius of $1.06^{+0.06}_{-0.05}\,R_\oplus$. HD 137010 b is therefore only marginally larger than Earth. To our knowledge, this is the smallest high-confidence planet candidate reported from a single transit around a Sun-like star; among all transiting exoplanets, it may be exceeded only by TRAPPIST-1 h, originally discovered from a single transit by Spitzer and with orbital period resolved by K2 (M. Gillon et al. 2017; R. Luger et al. 2017).

We may estimate the amount of stellar flux received by HD 137010 b relative to Earth using the following equation:

$$I = \frac{L_*}{a}, \tag{6}$$

where L_* is the stellar luminosity relative to the Sun and a is the planetary semimajor axis in astronomical unit. Given $L_* = 0.232^{+0.023}_{-0.021}\,L_\odot$ (Table 1) and $a = 0.88^{+0.32}_{-0.10}$ au, we estimate that HD 137010 b receives an incident flux of $I = 0.29^{+0.11}_{-0.13}$ times that which Earth receives from the Sun. Among the major solar system bodies this is most comparable to Mars, which receives $I = 0.43\,I_\oplus$. We plot the posterior distributions in orbital period and incident flux in Figure 5. While HD 137010 b appears to have a similar orbital period and radius to Earth, it is likely to be significantly cooler on account of its less luminous K-type host star. We discuss the implications of this in the following sections.

4. Discussion

4.1. System Properties

In this work, we have reported the discovery of HD 137010 b, an Earth-sized candidate planet detected in K2 transit photometry around a $V = 10$ K-dwarf star. Through detailed analysis of available observations of HD 137010, we have excluded all conventional hypotheses for the transit event other than a transiting exoplanet; however, confirmation of the planetary hypothesis will require observation of a second transit or another form of additional detection. While we therefore present HD 137010 b as a planet candidate, we anticipate there is a high likelihood that it is a genuine planet and we analyze it here as if it were confirmed as such.

We have performed a fit to the single transit of HD 137010 b assuming a zero-eccentricity planetary transit model. We estimate a radius of $1.06^{+0.06}_{-0.05}\,R_\oplus$ and an orbital period of 355^{+200}_{-59} days. To our knowledge, this is the smallest planet candidate detected from a single transit around a Sun-like star, and is particularly remarkable for its Earth-like radius and orbital properties. We discuss the temperature and potential habitability of HD 137010 b further in the following section (Section 4.2).

The discovery of HD 137010 b demonstrates the detectability of temperate and cool Earth-sized exoplanets orbiting Sun-like stars through single transits. However this has only been made possible thanks to an especially favorable set of circumstances, namely the exceptionally high precision of the K2 photometry (CDPP = ∼8.5 ppm, Section 2.1), and further facilitated by the subsolar radius of HD 137010. Whereas HD 137010 b has a transit depth of 225 ± 10 ppm, the transit of Earth across the Sun would have a depth of only ≈100 ppm; hence, while the transit of HD 137010 b has been detected with a white noise SNR = 30, an equivalent Earth transit would have less than half the SNR (≈14). Given that only a small fraction of solar-type stars observed by Kepler and K2 have

such precise photometry, it is perhaps unsurprising that no exoplanet similar to HD 137010 b has previously been reported from a single transit.

The HD 137010 system is notable in that it contains a long-period transiting terrestrial planet candidate without showing any evidence for additional terrestrial planets. We can largely exclude transiting planets larger than $\geqslant 1\,R_{\oplus}$ with orbital periods below $P < 30$ days (Section 3.2.1), which contrasts with known transiting exoplanet systems that contain multiple small planets extending from short periods out to the HZ (e.g., Kepler-62, Kepler-186; W. J. Borucki et al. 2013; E. V. Quintana et al. 2014). However, this does not necessarily mean that HD 137010 b is isolated. Due to the finite duration of K2 observations, the detectability of transiting planets declines toward longer periods, and for beyond the 88 days baseline of the K2 photometry it would be entirely possible for additionally planets to simply not be observed in transit.[12] There is therefore considerable space for additional planets of similar size interior or exterior to the orbit of HD 137010 b that could have gone undetected by K2, and we cannot assume that HD 137010 b is dynamically isolated. For example, it is entirely possible that a solar systemlike architecture, with multiple terrestrial planets in the region between 0.2 and 2 au, may simply have failed to produce more than one detectable transit during K2 observations. Alternatively, interplanet mutual inclinations larger than a few tenths of a degree could result in hypothetical other planets in the system to fail to transit altogether. Thus, while HD 137010 b currently appears to be isolated, it cannot be ruled out that there are additional terrestrial planets in the system that may be detected through further observations.

In Section 3.2.2, we analyzed archival HARPS RVs and Hipparcos–Gaia astrometry to constrain the existence of additional companions in the HD 137010 system. The most salient evidence for a third body is the $\sim 7\,\mathrm{m\,s^{-1}}$ drift in the HARPS RVs, which is nominally $>4\sigma$ significant and does not appear to be explained by stellar activity. Due to the limitations of the data, it is not possible to confidently determine the origin of this variation, but assuming it does originate from a third body, we may estimate a provisional companion mass as a function of projected separation, which we have shown in Figure 4. Though we can largely rule out the role of a stellar companion (at least above $\gtrsim 0.2\,M_{\odot}$) from our imaging and Gaia constraints, the acceleration could equally be reproduced by anything between a sub-Jovian planet within a few astronomical units to a brown dwarf at ≈ 50 au. However, given that brown dwarfs are rarer than giant planets around Sun-like stars (e.g., D. Grether & C. H. Lineweaver 2006), it appears most plausible a posteriori that the RV variation could originate from a giant planet with an orbit exterior to HD 137010 b. We note that at a projected separation of ≈ 5 au the trend would be consistent with an $\approx 1\,M_{\mathrm{J}}$ planet, properties comparable to Jupiter. While the available data is insufficient to draw definite conclusions on the existence and parameters of a third body, we reason that the existence of an additional planet orbiting HD 137010 is a plausible explanation for the RV variability and suggest that further RV observations may confirm this hypothesis.

[12] Given an orbital period of 355^{+200}_{-59} days, there is only a 25^{+5}_{-8}% probability that a transit of HD 137010 b occurred during the 88 days of K2 Campaign 15 observations.

If HD 137010 does additionally host an additional long-period companion, it would be significant for understanding the system context of HD 137010 b. Any third body that could reproduce the observed RV variability is likely to be more massive than the transiting planet candidate by multiple orders of magnitude, meaning that it would dominate the angular momentum budget of the planetary system. Dependent on its hypothetical orbital properties, a third body may have significant implications on the formation history of HD 137010 b; previous studies have suggested that there is a correlation between the incidence of short-period super-Earths and long-period giant planets (W. Zhu & Y. Wu 2018; M. L. Bryan et al. 2019), suggesting that the existence of giant planets significantly influences the formation of planets on interior orbits. Constraining the properties of the potential long-period companion of HD 137010 may therefore be an important avenue for further study of the system.

Finally, we note that transits of Earth would not be observed from the perspective of HD 137010 because its ecliptic latitude of $-1.^{\circ}06$ places it outside of the Earth transit zone, which is only $0.^{\circ}5$ wide (R. Heller & R. E. Pudritz 2016).

4.2. Potential Habitable Zone Orbit

At the conclusion of Section 3.4, we used our constraints on the planetary orbit and the stellar luminosity to estimate the relative amount of stellar flux incident on HD 137010 b. We found that this was equal to $I = 0.29^{+0.11}_{-0.13}\,I_{\oplus}$, which is significantly lower than the solar flux experienced by Earth and likely inferior to that of Mars ($0.43\,I_{\oplus}$). We may take this further by estimating the planetary equilibrium temperature through the following equation:

$$T_{\mathrm{eq}} = T_{\mathrm{eff},*}\sqrt{\frac{R_*}{2a}}\,(1-\alpha)^{1/4}, \tag{7}$$

where T_{eff} is the stellar effective temperature, R_* is the stellar radius, a is again the planetary semimajor axis in astronomical unit, and α is the bond albedo of the planet. Though the bond albedo is not known, we may vary through physically plausible values for this parameter in order to get a sense for the equilibrium temperature of HD 137010 b. Assuming a minimal bond albedo of $\alpha = 0.0$, the equilibrium temperature is $T_{\mathrm{eq}} = 205^{+17}_{-28}$ K (-68°C). Alternatively, assuming an "Earth-like" $\alpha = 0.3$, we find $T_{\mathrm{eq}} = 188^{+16}_{-25}$ K (-85°C).

It therefore appears likely that HD 137010 b is among the coolest Earth-sized transiting planets yet discovered orbiting a Sun-like star, and we are motivated to consider whether HD 137010 b lies in the HZ. Though the equilibrium temperature estimates above lie substantially below the 273 K freezing point of water, liquid water may still be facilitated given ideal atmospheric conditions. We follow the R. K. Kopparapu et al. (2013) model to define the circumstellar HZ. Adopting $T_{\mathrm{eff}} = 4770$ K and $L_* = 0.232^{+0.023}_{-0.021}\,L_{\odot}$ for HD 137010, we find that the the conservative bounds of the HZ are [0.48, 0.88] au ([1.00, 0.30] $I_{\oplus}$), whereas the optimistic limits are [0.38, 0.93] au ([1.60, 0.27] $I_{\oplus}$). Given the mass of HD 137010, this converts to conservative and optimistic limits in orbital period of [140, 350] days and [100, 380] days, respectively. We plot the R. K. Kopparapu et al. (2013) HZ limits over the orbital period and incident flux posterior distributions for HD 137010 b in Figure 5. HD 137010 b lies within the the conservative and optimistic HZ limits in 40%

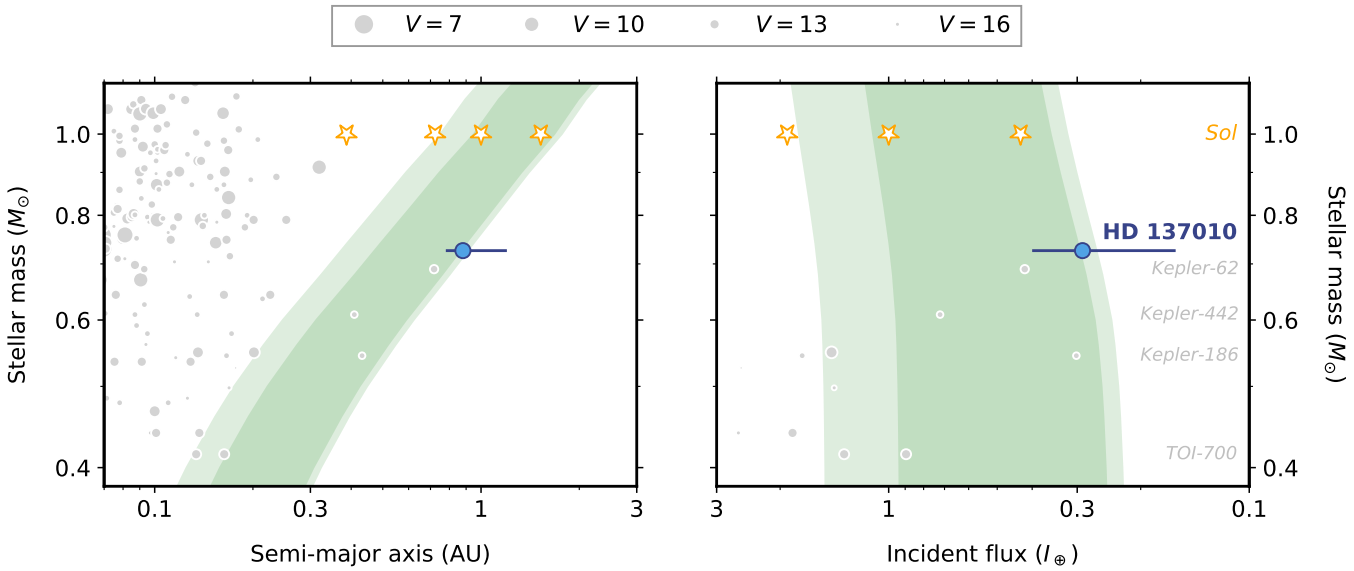


Figure 6. HD 137010 b in context. We plot known transiting planets smaller than $<1.6\,R_\oplus$ orbiting 0.4–1.2 $M_\odot$ stars with gray points in semimajor axis (left) and incident flux (right) space, with host star masses on the *y*-axis and point sizes scaled to *V*-band magnitude. We additionally highlight the solar system terrestrial planets using orange stars and mark the R. K. Kopparapu et al. (2013) HZ limits in green. Systems mentioned in the text are labeled on right. HD 137010 b is an exceptional example of an Earth-sized planet orbiting around the outer edge of the HZ of a bright Sun-like star.

and 51% of our transit models, respectively. All of the remaining posteriors lie beyond the HZ limits, so there is a ≈50% probability that HD 137010 b overshoots the R. K. Kopparapu et al. (2013) HZ.

The properties of HD 137010 b invite comparison to Kepler-186 f, the first-known Earth-sized exoplanet orbiting in the HZ (E. V. Quintana et al. 2014). Kepler-186 f has a radius of $1.11 \pm 0.14\,R_\oplus$ and receives a low incident flux of $0.320^{+0.059}_{-0.039}\,I_\oplus$ (E. V. Quintana et al. 2014). Though Kepler-186 is less massive than HD 137010 ($0.48\,M_\odot$ versus $0.73\,M_\odot$), Kepler-186 f nonetheless constitutes one of the closest analogs to HD 137010 b among known exoplanets. The potential habitability of Kepler-186 f was studied by E. Bolmont et al. (2014), who explored the surface temperatures of model planets with atmospheres composed of CO_2, N_2, and H_2O. Varying the CO_2 partial pressure under different planetary properties and N_2 abundances, they found that the surface temperature consistently rises above the 273 K freezing point of H_2O given 200–500 mbar of CO_2. Assuming that broadly similar outcomes would apply for HD 137010 b, it appears eminently plausible that a moderately CO_2-rich atmosphere would be conducive to liquid surface water.

However, a plausible alternative scenario is that the surface of HD 137010 b is frozen (a "snowball" climate). For a model Earth-like planet with a fixed modern CO_2 abundance, the results of E. T. Wolf et al. (2017) imply that for an early K-type host star snowball climate states develop where $I \lesssim 0.8\,I_\oplus$, which includes our entire posterior distribution. A fully glaciated planet would be highly reflective, significantly reducing the surface temperature. The later spectral type of HD 137010 has only a moderate effect on the high reflectivity of surface ice; according to C. Wilhelm et al. (2022), ice on an Earth-like planet orbiting an early K-dwarf has an albedo of 0.55, compared to 0.6 for a G-dwarf. Assuming a high bond albedo of $\alpha = 0.5$ from the Huronian snowball Earth model of A. D. Del Genio et al. (2019) to represent a fully glaciated planet, we derive $T_{\rm eq} = 173^{+14}_{-23}$ K (−100°C). The prospects for surface water and habitability are therefore highly dependent on atmospheric composition, particularly the relative abundance of CO_2.

4.3. HD 137010 b in Context

We place HD 137010 b in the context of known terrestrial planets in Figure 6. Here, we compare HD 137010 b to the solar system terrestrial planets and to known transiting exoplanets with $R_p < 1.6\,R_\oplus$. The radius cut is intended to limit our sample to terrestrial exoplanets because it is now conventional wisdom that planets larger than $>1.6\,R_\oplus$ are unlikely to be rocky (L. A. Rogers 2015).[13] We plot known planets in both semimajor axis and incident flux space as a function of stellar mass between 0.4 and $1.2\,M_\odot$. The aim of this stellar mass restriction is to approximately limit the sample to FGK-type stars, though we have extended the selection below $\leqslant 0.6\,M_\odot$ into the early M-dwarf range to enable comparison with the notable HZ planets TOI-700 d and e (M2V, $M_* = 0.42\,M_\odot$; E. A. Gilbert et al. 2020, 2023). We also plot the R. K. Kopparapu et al. (2013) HZ limits over both axes.

Figure 6 demonstrates that the region of parameter space occupied by HD 137010 b is otherwise largely barren. The most similar known exoplanet is Kepler-62 f which has $P = 267.3$ days, $a = 0.72$ au, $I = 0.41 \pm 0.05\,I_\oplus$, and $R_p = 1.41 \pm 0.07\,R_\oplus$ and orbits a K2V star (W. J. Borucki et al. 2013). Other transiting planets with comparable parameters include Kepler-442 b (G. Torres et al. 2015) and Kepler-186 f (E. V. Quintana et al. 2014), both orbiting lower mass stars. HD 137010 b is therefore a significant addition to the small sample of cool terrestrial planet candidates orbiting K-dwarf stars.

Compared to the other terrestrial HZ transiting planet candidates orbiting stars more massive than $\geqslant 0.6\,M_\odot$ in Figure 6, HD 137010 b can be distinguished from those

[13] We note that this radius cut leads to the marginal exclusion of the well-known HZ planets Kepler-62 e ($1.61 \pm 0.05\,R_\oplus$; W. J. Borucki et al. 2013) and Kepler-452 b ($1.63^{+0.23}_{-0.20}\,R_\oplus$; J. M. Jenkins et al. 2015).

previously known by its bright host star ($V = 10$). The aforementioned Kepler planets all orbit stars fainter than $V \geqslant 14$, sufficiently faint to preclude substantial characterization efforts with current instruments. Previous discoveries of terrestrial planets in the HZ of bright stars have been restricted to M-dwarfs. This has undoubtedly been facilitated by detectability biases given that HZ planets around M-dwarfs have shorter orbital periods and deeper transit signals. However, there are well-known concerns on the ability of terrestrial planets orbiting M-dwarfs to retain their atmospheres in the face of long-term exposure to high-energy radiation from their host stars (e.g., K. J. Zahnle & D. C. Catling 2017; E. K. Pass et al. 2025). Due to their shorter active lifetimes and the larger orbital separations of their HZs, there is a case to be made for the favorability of K-dwarfs to planetary habitability over M-dwarfs. Indeed, the habitability potential of planets orbiting early-to-mid K-dwarfs was highlighted as early as the foundational work of J. F. Kasting et al. (1993), and has been promoted both in the theoretical aspect (e.g., M. Cuntz & E. F. Guinan 2016) and also from the perspective of biosignature detectability (e.g., G. N. Arney 2019). HD 137010 b is the first example of a transiting terrestrial planet candidate orbiting in or near to the HZ of a K-type dwarf bright enough to allow for substantial follow-up observations, and may be of interest for future work on the habitability of K-dwarf planets.

4.4. Prospects for Confirmation

Though the single transit observed by K2 provides evidence for the existence of HD 137010 b, confirmation and further study both critically depend on redetection of the planetary signal. Here we explore the prospects for confirmation of HD 137010 b through various methods.

4.4.1. Transit

As HD 137010 b has already been detected in transit, this provides the most obvious avenue for redetection. However, the shallow transit depth means that such an observation would be beyond the capability of many instruments.

At present, the TESS mission (G. R. Ricker et al. 2014) presents the best prospects for redetection of the transit of HD 137010 b. However, TESS employs an observing strategy which generally avoids the ecliptic plane (G. R. Ricker et al. 2014). This minimizes the impact of scattered light from solar system bodies, but naturally also limits overlap with K2 targets. Nonetheless, in past regions of overlap, TESS reobservation of K2 targets have proved highly informative (e.g., E. Thygesen et al. 2023, 2024). Forays into the ecliptic have been made during the TESS extended mission, but until recently these have been restricted to the northern ecliptic.

However, TESS has recently executed its first sweep of the southern ecliptic, and observed HD 137010 for the first time in Sector 91 (2025 April–May). Extrapolating forwards from our orbital period posteriors, we estimated a ∼7% chance that a transit of HD 137010 b would occur during Sector 91. We proposed for TESS 20 s cadence observations for HD 137010 to maximize the photometric SNR. The TESS photometry has a CDPP of ∼42 ppm (compared to ∼8.5 ppm for K2), which makes detection of HD 137010 b challenging since the expected transit SNR would be ≈7. We do not observe any visually obvious transits in the TESS light curve that could be attributed to the K2 planet candidate, but it is not impossible that such a transit could evade detection given the photometric precision.

In the event that a second transit of HD 137010 b is detected, this would only constrain a maximum value of the orbital period and would leave the true orbital period as an undetermined alias of this value (see J. C. Becker et al. 2019; S. Dholakia et al. 2020). In this scenario, a possible avenue for resolving the true period would be to use CHEOPS (W. Benz et al. 2021). CHEOPS observations have been productively used to resolve period aliases of several planets originally detected by TESS (e.g., H. P. Osborn et al. 2022, 2023). Though the comparatively low transit incidence means that such an effort would be time-intensive, this may be the most viable path to confirm HD 137010 b and determine its orbital period.

A near-future mission of relevance is PLATO (H. Rauer et al. 2014, 2025). PLATO will search for Earth-sized transiting planets orbiting in the HZ using a long-duration "staring" pointing strategy reminiscent of Kepler. The properties of HD 137010 b align closely with planets expected to be detected (R. Heller et al. 2022). However, the planned locations of the PLATO long-pointing fields lie near to the ecliptic poles, and do not overlap with the ecliptic locations of the K2 fields (V. Nascimbeni et al. 2022). It therefore appears unlikely that PLATO could be used to specifically redetect the transit of HD 137010 b.

4.4.2. Radial Velocity

The radial velocity method is one of the main methods used for exoplanet discovery and mass measurement, and RV detection of exoplanets with Earth-like masses and periods has been a long-time goal in the field. We therefore consider the prospects for RV detection of HD 137010 b. If we assume that a $1.06^{+0.06}_{-0.05}\,R_\oplus$ planet has the same density as Earth, we would expect it to have a mass of $1.20^{+0.21}_{-0.15}\,M_\oplus$. Using our adopted stellar mass and orbital period and assuming zero orbital eccentricity, we calculate that the expected radial velocity semiamplitude for HD 137010 b given this mass would be $0.13 \pm 0.02\,\mathrm{m\,s^{-1}}$, which is comparable to the reflex signal of Earth. There are considerable challenges in RV planet detection for semiamplitudes much below the $<1\,\mathrm{m\,s^{-1}}$ level due to instrument limitations and stellar effects (ex. N. C. Hara & E. B. Ford 2023), and the expected 13 $\mathrm{cm\,s^{-1}}$ semiamplitude of HD 137010 b lies considerably below the smallest planetary RV signals detected so far.

We may establish a sense for the challenge of detecting HD 137010 b through comparison to past RV targets with similar observational properties. Here, we compare to previous RV observations of the star GJ 9827, which like HD 137010 is a 10th magnitude K-dwarf. GJ 9827 has a system of three short-period planets discovered by K2 (P. Niraula et al. 2017; J. E. Rodriguez et al. 2018) and has gained a substantial body of RV observations used to measure the masses of these planets, each of which have RV semiamplitudes of a few $\mathrm{m\,s^{-1}}$. The most recent RV results from V. M. Passegger et al. (2024), which included 54 RVs from the ESPRESSO spectrograph and a total of 167 RVs from preceding publications, achieved posterior uncertainties on the RV semiamplitudes of $\pm\sim0.25\ \mathrm{m\,s^{-1}}$ for the three planets. Detection of the RV signal expected from HD 137010 b is therefore likely to entail a larger number of observations with

higher precision, which would be challenging for current instruments.

Nonetheless, there is substantial interest in working toward the detection of the small RV signals of Earth analogs (see in particular J. Crass et al. 2021). We therefore highlight HD 137010 as a target of interest for current and future extreme-precision RV surveys. HD 137010 is the first Sun-like star with an Earth-sized HZ planet candidate that is also sufficiently bright for precise RV observations. It presents an advantage over blind selection of RV targets in that there is already evidence for a cool Earth-sized planet orbiting the star. Given the location of the star in the ecliptic (decl. = –20), it is accessible from most observatories with high-precision RV spectrographs. We also note that there is evidence for an additional companion in existing HARPS RV observations of HD 137010 with a longer orbital period (Section 3.2.2), which may be more easily detected with current instruments.

4.4.3. Astrometry

Astrometry has been raised as a potential method for the detection of Earth analogues. However, this largely lies beyond the capabilities of existing instruments. In the case of HD 137010 b, assuming a mass of $1.20^{+0.21}_{-0.15}\,M_{\oplus}$ as in the previous section we would anticipate an astrometric reflex signal with a semiamplitude of $\sim$0.1 μas. This is approximately two orders of magnitude below the astrometric precision of Gaia, which is around 10 μas (Gaia Collaboration et al. 2016). The Nancy Grace Roman Space Telescope may achieve an astrometric precision of 1–10 μas (WFIRST Astrometry Working Group et al. 2019), which is still significantly larger than the expected signal.

Various space mission concepts for the astrometric detection of exoplanets have been proposed over the years (see M. Janson et al. 2018). Recent mission proposals aiming for the detection of HZ exoplanets using sub-μas precision astrometry include Theia (The Theia Collaboration et al. 2017) and CHES (J.-H. Ji et al. 2022). HD 137010 b may be a target of interest for astrometric exoplanet detection efforts.

4.4.4. Imaging

In recent years, there has been significant exploration of the near-future potential for the detection of Earth analogues with direct imaging. A highlight of this is the NASA Habitable Worlds Observatory (HWO) mission recommended in the Astro2020 decadal survey (National Academies of Sciences, Engineering, and Medicine 2021), which aims to image Earth-like planets orbiting nearby stars using a space-based coronagraphic instrument.

HD 137010 b lies closer to the parameter space intended to be explored by HWO than almost any known transiting HZ exoplanet. With an estimated physical semimajor axis of $0.88^{+0.32}_{-0.10}$ au at a distance of 44.86 $\pm$ 0.03 pc, we estimate that HD 137010 b has a projected semimajor axis of 20^{+7}_{-2} mas.[14] However, this may still be too small of a separation to facilitate direct detection. The requirements for stellar target selection for HWO has been explored by E. Mamajek & K. Stapelfeldt (2024), and while the inner working angle (IWA) of the instrument has not yet been defined, this projected separation is around a factor of 3–4 smaller than the "Tier C" target IWA constraint (approximately 70 mas; E. Mamajek & K. Stapelfeldt 2024, Figure 1). This means that, with due allowance for the yet-to-be finalized instrument design, it appears likely that HD 137010 b will be too close to its host star to be detected with HWO.

A second mission concept aiming for the direct detection of Earth-like exoplanets is the Large Interferometer For Exoplanets (LIFE; S. P. Quanz et al. 2022). While likewise optimized for the detection planets around nearby stars (S. P. Quanz et al. 2022 consider stars within <20 pc), the nulling interferometer design means that it would not have a strict IWA in contrast to a coronagraphic instrument. Depending on the planetary properties, LIFE may therefore be capable of imaging HD 137010 b; this is a potential avenue for exploration in future work.

5. Conclusions

In this work, we have presented the discovery of HD 137010 b, an Earth-sized transiting planet candidate detected from a single transit observed in K2 Campaign 15 on the $V = 10.1$ K3.5V star HD 137010. A comprehensive analysis of the K2 observations, historical low-resolution imaging and new high-resolution speckle imaging data, archival HARPS RVs, and Hipparcos–Gaia astrometry allow us to exclude the conventional false-positive hypotheses for the transit signal, leaving a transiting exoplanet as the most plausible explanation for the photometric event. However, since we only have the evidence of one transit event, we ultimately classify HD 137010 b as a candidate planet.

We have implemented a single-transit exoplanet model to fit the transit of HD 137010 b. We determine that it has a radius of $1.06^{+0.06}_{-0.05}\,R_{\oplus}$, and assuming negligible orbital eccentricity, an orbital period of 355^{+200}_{-59} days (semimajor axis of $0.88^{+0.32}_{-0.10}$ au). While these properties are remarkably similar to Earth, due to the subsolar luminosity of HD 137010, we estimate that the candidate planet receives an incident flux of $I = 0.29^{+0.11}_{-0.13}\,I_{\oplus}$ which may be less than the flux received by Mars. Following the R. K. Kopparapu et al. (2013) definitions for the conservative and optimistic HZ, we find that there is a 40% probability that HD 137010 b lies within the conservative limits and a 51% probability that it falls within the optimistic HZ; all remaining solutions place it beyond the outer limits. If it does fall within the HZ, a moderately CO_2-rich atmospheric composition may allow for the formation of liquid surface water, whereas a CO_2 abundance more similar to Earth might instead result in a frozen "snowball" climate.

HD 137010 b is essentially unique as a candidate terrestrial HZ planet transiting a bright Sun-like star. We encourage follow-up observations for the confirmation and characterization of HD 137010 b, and to better understand the architecture of the system.

Acknowledgments

We acknowledge and pay respect to Australia's Aboriginal and Torres Strait Islander peoples, who are the traditional custodians of the lands, waterways, and skies all across Australia. We thank the anonymous referee for their helpful comments, which have helped to improve this work. A.Ve. thanks Mary Anne Limbach for thought-provoking discussion

[14] We note that since it is transiting and the orbital inclination is near to 90°, the semimajor axis represents the maximum value for the projected separation, and HD 137010 b would necessarily spend a significant fraction of its orbit at smaller separations.

(and earnest enthusiasm) which helped to improve this work. A.Ve. and C.X.H. are supported by ARC DECRA project DE200101840.

We acknowledge all efforts which went into the Planet Hunters citizen science project throughout the Kepler and K2 missions, in the absence of which this work would not have been possible.

This research is based on observations collected at the European Southern Observatory under ESO programs 072.C-0488(E) and 085.C-0019(A). This research has made use of the SIMBAD database and VizieR catalog access tool, operated at CDS, Strasbourg, France. This research has made use of NASA's Astrophysics Data System. This Letter includes data collected by the Kepler mission. Funding for the Kepler mission is provided by the NASA Science Mission directorate. Some of the data presented in this Letter were obtained from the Mikulski Archive for Space Telescopes (MAST). STScI is operated by the Association of Universities for Research in Astronomy, Inc., under NASA contract NAS5–26555. Support for MAST for non-HST data is provided by the NASA Office of Space Science via grant NNX13AC07G and by other grants and contracts.

Facilities: Kepler (K2), TESS, Hipparcos, Gaia, Gemini: South (Zorro), ESO:3.6m (HARPS).

Software: `emcee` (D. Foreman-Mackey et al. 2013), `batman` (L. Kreidberg 2015), `Vartools` (J. D. Hartman & G. Á. Bakos 2016), `LcTools` (A. R. Schmitt et al. 2019), `minimint` (S. Koposov 2021), `kiauhoku` (J. Tayar et al. 2022).

Appendix A
Data

In this section, we present the data used in this work.

In Table 3, we present the K2 photometry used in this work. See Section 2.1 for further information.

In Table 4, we tabulate the HARPS observations of HD 137010 extracted from the ESO archive. We have converted all units from km s^{-1} to m s^{-1}, but have not otherwise altered the data.

Table 3
K2 Photometry of HD 137010

BJD - 2454833	Normalized Flux	Detrended Flux
3157.8752	0.99945683	1.0000828
3157.8956	0.99943504	1.0000273
3157.9160	0.99941655	0.99997813
3157.9365	0.99945957	0.99999344
3157.9569	0.99948045	0.99998964
...	...	...
3244.3222	0.99972678	1.0000044
3244.3426	0.99972075	0.99999964
3244.3630	0.99970085	0.99998146
3244.3835	0.99971981	1.0000025
3244.4243	0.99971669	1.0000050

Note.

(This table is available in its entirety in machine-readable form in the online article.)

Table 4
HARPS Radial Velocity Data for HD 137010

BJD	RV (m s^{-1})	RV Error (m s^{-1})	Bisector span (m s^{-1})
2453834.84478	27931.19	1.34	6.20
2453835.79152	27933.31	1.22	13.21
2453979.53447	27931.19	1.99	19.52
2453982.49629	27930.73	1.39	6.77
2455268.89844	27937.27	1.13	18.35
2455298.76206	27936.37	1.74	13.48
2455306.77737	27938.23	1.36	10.51
2455307.78489	27940.56	1.10	18.90

Table 5
Proper Motion Data for HD 137010 Extracted from the Hipparcos–Gaia Catalog of Accelerations

Measurement	μ_α (mas yr^{-1})	μ_δ (mas yr^{-1})
Hipparcos	229.991 ± 2.082	−248.313 ± 1.878
Gaia EDR3	228.536 ± 0.028	−248.158 ± 0.019
Hipparcos–Gaia	228.533 ± 0.068	−248.183 ± 0.050

In Table 5, we present the Hipparcos–Gaia astrometry for HD 137010, as extracted from Gaia EDR3 version of the Hipparcos–Gaia Catalog of Accelerations (T. D. Brandt 2021). We refer the reader to T. D. Brandt (2018, 2021) and further to T. D. Brandt et al. (2019) for a full description of this data. We note for clarity that the astrometric solution for HD 137010 is unchanged between Gaia EDR3 and Gaia DR3.

In Figure 7, we present the Zorro speckle imaging observations of HD 137010 discussed in Section 2.4. Observations were taken in the 562 nm and 832 nm filters on 2024 July 12. No additional sources were detected above the 5σ contrast limits.

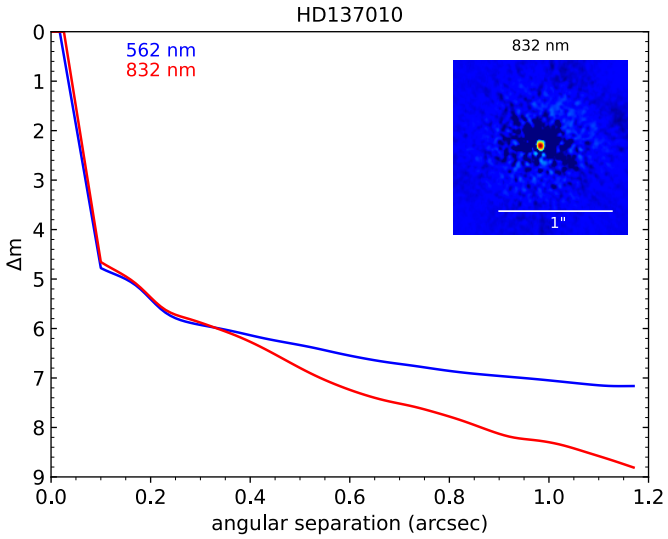


Figure 7. Zorro speckle imaging observations of HD 137010 obtained on 2024 July 12. The red and blue contrast curves represent the 5σ contrast limits as a function of projected separation at 832 nm and 562 nm, respectively. The inset figure shows the reconstructed 832 nm image. No additional sources are detected.

Appendix B
Isochrone Model

Here, we detail the data and priors used in our isochrone model. As input data, we have used photometry from Tycho-2 (E. Høg et al. 2000), Gaia DR3 (Gaia Collaboration et al. 2023), 2MASS (M. F. Skrutskie et al. 2006), and WISE (specifically AllWISE; R. M. Cutri et al. 2012). We list the photometry in Table 6. We have applied a floor of ± 0.02 mag on the Gaia photometric precision.

We use `minimint` S. Koposov (2021) for isochrone interpolation and `emcee` (D. Foreman-Mackey et al. 2013) to sample the posterior space. Model variables include the stellar parallax, age, mass, $T_{\rm eff}$, $\log g$, and [Fe/H]; all are fitted log-linearly except for the last two, which are already logarithmic. As priors, we utilize the Gaia DR3 parallax ($\varpi = 22.292 \pm 0.017$ mas; Gaia Collaboration et al. 2023) and $T_{\rm eff} = 4797 \pm 121$ K, $[{\rm Fe/H}] = -0.22 \pm 0.07$ dex as derived from the HARPS spectra (S. G. Sousa et al. 2011). Following Section 3.1.1, we impose an upper bound on the stellar age of $<$10 Gyr, and utilize the age posterior from the M. J. Veyette & P. S. Muirhead (2018) *UVW*-age relationship as a prior for the model. This helps to penalize implausibly high model ages ($>$10 Gyr), which otherwise have a modest impact on the mass and density estimation. Due to the close proximity of HD 137010, we assume zero interstellar extinction.

The posteriors from our isochrone model are recorded in Table 1. In comparison to the spectroscopic priors, the addition of photometry affords a slight improvement in the precision on the effective temperature ($T_{\rm eff} = 4770 \pm 90$ K), but unsurprisingly no change for the [Fe/H]. The age posterior also closely reproduces the M. J. Veyette & P. S. Muirhead (2018) prior.

Our isochrone model natively returns a stellar mass of $M = 0.726 \pm 0.012\,M_{\odot}$. Reassuringly, this is in $\sim 1\sigma$ agreement with the mass of $0.709 \pm 0.013\,M_{\odot}$ previously reported by S. G. Sousa et al. (2011). However, this neglects the contribution to the error budget arising from systematic differences between stellar models, which should not be ignored at this level of precision. We use `kiauhoku` (J. Tayar et al. 2022) to quasi-empirically estimate the systematic uncertainty on the stellar mass through comparison of the outputs of different stellar models. `kiauhoku` returns a 1.7% systematic uncertainty on the stellar mass ($\pm 0.012\,M_{\odot}$), which when added in quadrature results in a final value of $0.726 \pm 0.017\,M_{\odot}$ for HD 137010. This is the posterior value recorded in Table 1 and adopted throughout this work. We have also propagated the increased mass uncertainty through to the stellar density and surface gravity.

Table 6
Photometry of HD 137010 Used by Our Isochrone Model

Band	Magnitude (mag)	References
$B_{\rm T}$	11.310 ± 0.091	E. Høg et al. (2000)
$V_{\rm T}$	10.245 ± 0.053	E. Høg et al. (2000)
G	9.706 ± 0.02	Gaia Collaboration et al. (2023)
$G_{\rm BP}$	10.260 ± 0.02	Gaia Collaboration et al. (2023)
$G_{\rm RP}$	9.004 ± 0.02	Gaia Collaboration et al. (2023)
J	8.162 ± 0.018	M. F. Skrutskie et al. (2006)
H	7.648 ± 0.031	M. F. Skrutskie et al. (2006)
K_S	7.526 ± 0.020	M. F. Skrutskie et al. (2006)
$W1$	7.456 ± 0.035	R. M. Cutri et al. (2012)
$W2$	7.525 ± 0.021	R. M. Cutri et al. (2012)
$W3$	7.506 ± 0.018	R. M. Cutri et al. (2012)
$W4$	7.670 ± 0.184	R. M. Cutri et al. (2012)

ORCID iDs

Alexander Venner https://orcid.org/0000-0002-8400-1646
Andrew Vanderburg https://orcid.org/0000-0001-7246-5438
Chelsea X. Huang https://orcid.org/0000-0003-0918-7484
Shishir Dholakia https://orcid.org/0000-0001-6263-4437
Hans Martin Schwengeler https://orcid.org/0000-0002-1637-2189
Steve B. Howell https://orcid.org/0000-0002-2532-2853
Robert A. Wittenmyer https://orcid.org/0000-0001-9957-9304
Martti H. Kristiansen https://orcid.org/0000-0002-2607-138X
Ivan A. Terentev https://orcid.org/0000-0002-0654-4442

References

Adibekyan, V. Z., Sousa, S. G., Santos, N. C., et al. 2012, A&A, 545, A32
Almeida-Fernandes, F., & Rocha-Pinto, H. J. 2018, MNRAS, 476, 184
Arney, G. N. 2019, ApJL, 873, L7
Becker, J. C., Vanderburg, A., Rodriguez, J. E., et al. 2019, AJ, 157, 19
Bensby, T., Feltzing, S., & Lundström, I. 2003, A&A, 410, 527
Benz, W., Broeg, C., Fortier, A., et al. 2021, ExA, 51, 109
Bolmont, E., Raymond, S. N., von Paris, P., et al. 2014, ApJ, 793, 3
Borucki, W. J., Koch, D. G., Batalha, N., et al. 2012, ApJ, 745, 120
Borucki, W. J., Koch, D., Basri, G., et al. 2010, Sci, 327, 977
Borucki, W. J., Agol, E., Fressin, F., et al. 2013, Sci, 340, 587
Bowler, B. P., Cochran, W. D., Endl, M., et al. 2021, AJ, 161, 106
Brandt, T. D. 2018, ApJS, 239, 31
Brandt, T. D. 2021, ApJS, 254, 42
Brandt, T. D., Dupuy, T. J., & Bowler, B. P. 2019, AJ, 158, 140
Bryan, M. L., Knutson, H. A., Lee, E. J., et al. 2019, AJ, 157, 52
Burke, C. J., Mullally, F., Thompson, S. E., Coughlin, J. L., & Rowe, J. F. 2019, AJ, 157, 143
Choi, J., Dotter, A., Conroy, C., et al. 2016, ApJ, 823, 102
Claret, A. 2018, A&A, 618, A20
Coughlin, J. L., Thompson, S. E., Bryson, S. T., et al. 2014, AJ, 147, 119
Crass, J., Gaudi, B. S., Leifer, S., et al. 2021, arXiv:2107.14291
Cuntz, M., & Guinan, E. F. 2016, ApJ, 827, 79
Cutri, R. M., Skrutskie, M. F., van Dyk, S., et al. 2012, yCat, 2281, 0
Dalba, P. A., Kane, S. R., Dragomir, D., et al. 2022, AJ, 163, 61
Del Genio, A. D., Kiang, N. Y., Way, M. J., et al. 2019, ApJ, 884, 75
Dholakia, S., Dholakia, S., Mayo, A. W., & Dressing, C. D. 2020, AJ, 159, 93
Dholakia, S., Palethorpe, L., Venner, A., et al. 2024, MNRAS, 531, 1276
Dotter, A. 2016, ApJS, 222, 8
Dragomir, D., Teske, J., Günther, M. N., et al. 2019, ApJL, 875, L7
Dransfield, G., Timmermans, M., Triaud, A. H. M. J., et al. 2024, MNRAS, 527, 35
Eisner, N. L., Barragán, O., Lintott, C., et al. 2021, MNRAS, 501, 4669
El-Badry, K., Rix, H.-W., & Heintz, T. M. 2021, MNRAS, 506, 2269
Foreman-Mackey, D., Hogg, D. W., Lang, D., & Goodman, J. 2013, PASP, 125, 306
Foreman-Mackey, D., Morton, T. D., Hogg, D. W., Agol, E., & Schölkopf, B. 2016, AJ, 152, 206
Fuhrmann, K. 2011, MNRAS, 414, 2893
Gaia Collaboration, Prusti, T., de Bruijne, J. H. J., et al. 2016, A&A, 595, A1
Gaia Collaboration, Vallenari, A., Brown, A. G. A., et al. 2023, A&A, 674, A1
Ge, J., Zhang, H., Zang, W., et al. 2022, arXiv:2206.06693
Gilbert, E. A., Barclay, T., Schlieder, J. E., et al. 2020, AJ, 160, 116
Gilbert, E. A., Vanderburg, A., Rodriguez, J. E., et al. 2023, ApJL, 944, L35
Giles, H. A. C., Osborn, H. P., Blanco-Cuaresma, S., et al. 2018, A&A, 615, L13
Gilliland, R. L., Chaplin, W. J., Dunham, E. W., et al. 2011, ApJS, 197, 6
Gillon, M., Triaud, A. H. M. J., Demory, B.-O., et al. 2017, Natur, 542, 456
Gomes da Silva, J., Santos, N. C., Adibekyan, V., et al. 2021, A&A, 646, A77
Gray, R. O., Corbally, C. J., Garrison, R. F., et al. 2006, AJ, 132, 161
Grether, D., & Lineweaver, C. H. 2006, ApJ, 640, 1051
Hara, N. C., & Ford, E. B. 2023, AnRSA, 10, 623
Hartman, J. D., & Bakos, G. Á. 2016, A&C, 17, 1
Heller, R., Harre, J.-V., & Samadi, R. 2022, A&A, 665, A11
Heller, R., & Pudritz, R. E. 2016, AsBio, 16, 259
Høg, E., Fabricius, C., Makarov, V. V., et al. 2000, A&A, 355, L27

Howell, S. B. 2020, The NASA Kepler Mission (Bristol: IOP Publishing)
Howell, S. B., Everett, M. E., Horch, E. P., et al. 2016, ApJL, 829, L2
Howell, S. B., Everett, M. E., Sherry, W., Horch, E., & Ciardi, D. R. 2011, AJ, 142, 19
Howell, S. B., Sobeck, C., Haas, M., et al. 2014, PASP, 126, 398
Howell, S. B., Martínez-Vázquez, C. E., Furlan, E., et al. 2025, FrASS, 12, 1608411
Huber, D., Bryson, S. T., Haas, M. R., et al. 2016, ApJS, 224, 2
Incha, E., Vanderburg, A., Jacobs, T., et al. 2023, MNRAS, 523, 474
Janson, M., Brandeker, A., Boehm, C., & Martins, A. K. 2018, in Handbook of Exoplanets, ed. H. J. Deeg & J. A. Belmonte (Berlin: Springer), 87
Jenkins, J. M., Twicken, J. D., Batalha, N. M., et al. 2015, AJ, 150, 56
Ji, J.-H., Li, H.-T., Zhang, J.-B., et al. 2022, RAA, 22, 072003
Johnson, D. R. H., & Soderblom, D. R. 1987, AJ, 93, 864
Kane, S. R., Ciardi, D. R., Gelino, D. M., & von Braun, K. 2012, MNRAS, 425, 757
Kasting, J. F., Whitmire, D. P., & Reynolds, R. T. 1993, Icar, 101, 108
Kipping, D. 2018, RNAAS, 2, 223
Kipping, D., Solano-Oropeza, D., Yahalomi, D. A., et al. 2025, NatAs, Advanced Online Publication
Koch, D. G., Borucki, W. J., Basri, G., et al. 2010, ApJL, 713, L79
Koposov, S. 2021, segasai/minimint: Minimint v0.3.0, Zenodo: doi:10.5281/zenodo.5610692
Kopparapu, R. K., Ramirez, R., Kasting, J. F., et al. 2013, ApJ, 765, 131
Kovács, G., Zucker, S., & Mazeh, T. 2002, A&A, 391, 369
Kreidberg, L. 2015, PASP, 127, 1161
Kristiansen, M. H. K., Rappaport, S. A., Vanderburg, A. M., et al. 2022, PASP, 134, 074401
Kunimoto, M., & Matthews, J. M. 2020, AJ, 159, 248
Kunimoto, M., Lin, Z., Millholland, S., et al. 2025, AJ, 169, 47
Kuzuhara, M., Fukui, A., Livingston, J. H., et al. 2024, ApJL, 967, L21
Lo Curto, G., Mayor, M., Benz, W., et al. 2010, A&A, 512, A48
Luger, R., Agol, E., Kruse, E., et al. 2016, AJ, 152, 100
Luger, R., Sestovic, M., Kruse, E., et al. 2017, NatAs, 1, 0129
Mamajek, E., & Stapelfeldt, K. 2024, arXiv:2402.12414
Mandel, K., & Agol, E. 2002, ApJL, 580, L171
Mann, C. R., Dalba, P. A., Lafrenière, D., et al. 2023, AJ, 166, 239
Mayor, M., Pepe, F., Queloz, D., et al. 2003, Msngr, 114, 20
Mullally, F., Thompson, S. E., Coughlin, J. L., Burke, C. J., & Rowe, J. F. 2018, AJ, 155, 210
Nascimbeni, V., Piotto, G., Börner, A., et al. 2022, A&A, 658, A31
National Academies of Sciences, Engineering, and Medicine 2021, Pathways to Discovery in Astronomy and Astrophysics for the 2020s (Washington, DC: The National Academies Press)
Niraula, P., Redfield, S., Dai, F., et al. 2017, AJ, 154, 266
Osborn, H. P., Armstrong, D. J., Brown, D. J. A., et al. 2016, MNRAS, 457, 2273
Osborn, H. P., Bonfanti, A., Gandolfi, D., et al. 2022, A&A, 664, A156
Osborn, H. P., Nowak, G., Hébrard, G., et al. 2023, MNRAS, 523, 3069
Pass, E. K., Charbonneau, D., & Vanderburg, A. 2025, ApJL, 986, L3
Passegger, V. M., Suárez Mascareño, A., Allart, R., et al. 2024, A&A, 684, A22
Perryman, M. A. C., Lindegren, L., Kovalevsky, J., et al. 1997, A&A, 323, L49
Quanz, S. P., Ottiger, M., Fontanet, E., et al. 2022, A&A, 664, A21
Quintana, E. V., Barclay, T., Raymond, S. N., et al. 2014, Sci, 344, 277
Rauer, H., Aerts, C., Cabrera, J., et al. 2025, ExA, 59, 26
Rauer, H., Catala, C., Aerts, C., et al. 2014, ExA, 38, 249
Ricker, G. R., Winn, J. N., Vanderspek, R., et al. 2014, Proc. SPIE, 9143, 914320
Robin, A. C., Reylé, C., Derrière, S., & Picaud, S. 2003, A&A, 409, 523
Rodriguez, J. E., Vanderburg, A., Eastman, J. D., et al. 2018, AJ, 155, 72
Rodriguez, J. E., Vanderburg, A., Zieba, S., et al. 2020, AJ, 160, 117
Rogers, L. A. 2015, ApJ, 801, 41
Rowe, J. F., Bryson, S. T., Marcy, G. W., et al. 2014, ApJ, 784, 45
Sandford, E., Espinoza, N., Brahm, R., & Jordán, A. 2019, MNRAS, 489, 3149
Schmitt, A. R., Hartman, J. D., & Kipping, D. M. 2019, arXiv:1910.08034
Schmitt, J. R., Tokovinin, A., Wang, J., et al. 2016, AJ, 151, 159
Schönrich, R., Binney, J., & Dehnen, W. 2010, MNRAS, 403, 1829
Scott, M. G., Triaud, A. H. M. J., Barkaoui, K., et al. 2025, MNRAS, 540, 1909
Scott, N. J., Howell, S. B., Gnilka, C. L., et al. 2021, FrASS, 8, 138
Sgro, L. A., Dalba, P. A., Esposito, T. M., et al. 2024, AJ, 168, 26
Skrutskie, M. F., Cutri, R. M., Stiening, R., et al. 2006, AJ, 131, 1163
Soubiran, C., Jasniewicz, G., Chemin, L., et al. 2018, A&A, 616, A7
Sousa, S. G., Santos, N. C., Israelian, G., Mayor, M., & Udry, S. 2011, A&A, 533, A141
Tayar, J., Claytor, Z. R., Huber, D., & van Saders, J. 2022, ApJ, 927, 31
The Theia Collaboration, Boehm, C., Krone-Martins, A., et al. 2017, arXiv:1707.01348
Thygesen, E., Ranshaw, J. A., Rodriguez, J. E., et al. 2023, AJ, 165, 155
Thygesen, E., Rodriguez, J. E., de Beurs, Z. L., et al. 2024, AJ, 168, 161
Torres, G., Kipping, D. M., Fressin, F., et al. 2015, ApJ, 800, 99
Uehara, S., Kawahara, H., Masuda, K., Yamada, S., & Aizawa, M. 2016, ApJ, 822, 2
van Leeuwen, F. 2007, A&A, 474, 653
Vanderburg, A., Becker, J. C., Kristiansen, M. H., et al. 2016b, ApJL, 827, L10
Vanderburg, A., Huang, C. X., Rodriguez, J. E., et al. 2019, ApJL, 881, L19
Vanderburg, A., & Johnson, J. A. 2014, PASP, 126, 948
Vanderburg, A., Latham, D. W., Buchhave, L. A., et al. 2016a, ApJS, 222, 14
Vanderburg, A., Mann, A. W., Rizzuto, A., et al. 2018, AJ, 156, 46
Vanderburg, A., Montet, B. T., Johnson, J. A., et al. 2015, ApJ, 800, 59
Venner, A., An, Q., Huang, C. X., et al. 2024, MNRAS, 535, 90
Venner, A., Vanderburg, A., & Pearce, L. A. 2021, AJ, 162, 12
Veyette, M. J., & Muirhead, P. S. 2018, ApJ, 863, 166
Wang, J., Fischer, D. A., Barclay, T., et al. 2015, ApJ, 815, 127
WFIRST Astrometry Working Group, Sanderson, R. E., Bellini, A., et al. 2019, JATIS, 5, 044005
Wilhelm, C., Barnes, R., Deitrick, R., & Mellman, R. 2022, PSJ, 3, 13
Wolf, E. T., Shields, A. L., Kopparapu, R. K., Haqq-Misra, J., & Toon, O. B. 2017, ApJ, 837, 107
Xiang, M., Liu, X., Shi, J., et al. 2017, ApJS, 232, 2
Zahnle, K. J., & Catling, D. C. 2017, ApJ, 843, 122
Zhu, W., & Wu, Y. 2018, AJ, 156, 92